Revised Parameters for the AMOEBA Polarizable Atomic Multipole Water Model

Marie L. Laury[#][§], **Lee-Ping Wang**[#][‡], **Vijay S. Pande**[‡], **Teresa Head-Gordon**[¶], and **Jay W. Ponder**[§]

[§]Department of Chemistry, Washington University in St. Louis, St. Louis, MO 63105

[‡]Department of Chemistry, Stanford University, Stanford, CA 94305

[¶]Department of Chemistry, University of California, Berkeley, CA 94720

[#] These authors contributed equally to this work.

Abstract

A set of improved parameters for the AMOEBA polarizable atomic multipole water model is developed. The protocol uses an automated procedure, ForceBalance, to adjust model parameters to enforce agreement with *ab initio*-derived results for water clusters and experimentally obtained data for a variety of liquid phase properties across a broad temperature range. The values reported here for the new AMOEBA14 water model represent a substantial improvement over the previous AMOEBA03 model. The new AMOEBA14 water model accurately predicts the temperature of maximum density and qualitatively matches the experimental density curve across temperatures ranging from 249 K to 373 K. Excellent agreement is observed for the AMOEBA14 model in comparison to a variety of experimental properties as a function of temperature, including the 2nd virial coefficient, enthalpy of vaporization, isothermal compressibility, thermal expansion coefficient and dielectric constant. The viscosity, self-diffusion constant and surface tension are also well reproduced. In comparison to high-level *ab initio* results for clusters of 2 to 20 water molecules, the AMOEBA14 model yields results similar to the AMOEBA03 and the direct polarization iAMOEBA models. With advances in computing power, calibration data, and optimization techniques, we recommend the use of the AMOEBA14 water model for future studies employing a polarizable water model.

INTRODUCTION

"What does a fish know about the water in which he swims all his life?"

~Albert Einstein ("Self Portrait", 1936)

"Water is the most extraordinary substance! Practically all its properties are anomalous…"

Corresponding Author: Jay W. Ponder, Department of Chemistry, Washington University in Saint Louis, Saint Louis, MO 63105, (314) 935-4275, ponder@dasher.wustl.edu.

~Albert Szent-Georgi ("The Living State", 1972)

Empirical models of water play an important role in the prediction and rationalization of bulk water properties. One of the first water models was proposed by Bernal and Fowler in 1933.[1] Before the advent of digital computers, this simple atomistic model was used to deduce the crystal structure of ice, X-ray diffraction curve for water, and the heat of solution of ions. Water was among the first molecular systems to be simulated at the atomic level via Monte Carlo[2] and molecular dynamics techniques.[3] The ST2 water model, used throughout much of the early computational work, showed simple distributed point charge models could be tailored to reproduce bulk properties.[4] Elaboration of fixed point charge models led to the development of the widely used TIP3P[2], TIP4P[2] and SPC[5] potentials, as well as the subsequent ST4[6], TIP5P[7], SPC/E[8], TIP4P-Ew[9] and F3C[10] potentials, among many others. All of these water models have been used as the foundation for development of various biomolecular force fields, therefore, many of the models are still commonly used for explicit solvent calculations on biological systems.

A tremendous variety of specialized water potentials have been proposed for accurate modeling of molecular cluster data and selected bulk properties. These specialized potentials are typically parameterized and calibrated against accurate and reliable *ab initio* results for small numbers of molecules and include an explicit accounting of electronic polarization. Perhaps the first pair-interaction water model to be systematically constructed from *ab initio* data was the original MCY model from 1976.[11] Early attempts at polarizable models include Vesely's work with Stockmayer potentials[12] and the polarizable electropole model of Barnes, *et al*.[13] Kuwajima and Warshel later incorporated explicit polarization into a modified potential inspired by the MCY work.[14] Other early polarizable potentials were provided by Sprik and Klein,[15] the NEMO method,[16] the POL3 model from Kollman's group,[17] and Dykstra's MMC model.[18] While a complete list is far too long to present here, more recent members extending this class would include TTM3-F,[19] SWM4-DP,[20] DPP2,[21] *etc*. Key features of such water models include the ability to reproduce with high fidelity the electrostatic potential around an isolated water molecule, and the ability of individual molecules to respond to their local environment. Some water potentials, such as TTM3, couple the electrostatic representation to the structure of the molecule as specified by valence terms. While potentials explicitly allowing proton dissociation were proposed over 35 years ago,[22] such models are not commonly used in molecular simulation.[23,24]

Much of chemistry can be rationalized at the level of partial charge interactions based on electronegativity arguments and inductive effects. To yield an accurate representation of an electrostatic potential usually requires a molecular description beyond simple partial atomic charges.[25] While atom-centered charge fitting schemes such as RESP[26] are extensively employed to parameterize force fields, the typical result is a relative error of several percent over an envelope close to, but outside of, the van der Waals surface of a polar molecule. One solution to improve upon the partial atomic charge water models is to include polarizability, as in the Atomic Multipole Optimized Energetics for Biomolecular Applications (AMOEBA) force field. The advantages of a polarizable model are evident in heterogeneous systems; for example, water-ion mixtures. Both cations and anions are highly polarizing, and the larger anions in particular are also very polarizable. While it is certainly possible for

non-polarizable force fields to provide reasonable bulk phase structural and thermodynamic properties,[27] a fully polarizable model should have an advantage in terms of transferability. Ion parameters derived against gas phase ion-water *ab initio* calculations adapt seamlessly to condensed phase modeling.[28]

The choice of water potential is often a key first step in construction of a general-purpose molecular force field. Water is a ubiquitous solvent, and the balance of solvent-solvent, solvent-solute and solute-solute interactions often plays a critical role in determining solute behavior. Computation of relative hydration free energies and ligand binding energies is aided by cancellation of errors in force field models. However, accurate calculation of absolute free energies generally requires a fine balance between solvent and solute interactions. Errors in the solvent-solvent potential will systematically recur in all subsequent calculations involving solvent. This explains the fact the most current biomolecular force fields are explicitly or implicitly parameterized for use with a particular water model. For example, recent revision of the Amber non-polarizable force field for use with the TIP4P-Ew water model involved a substantial reworking of the protein parameter values[29] or the elimination of the simple mixing rules to combine these force fields by explicitly parameterizing for the solute-solvent interactions themselves[30].

Fitting of model parameters can be carried out manually via a trial and error method, or an automated procedure can be employed. Least squares optimization of force fields first began with the Consistent Force Field proposed by Lifson and Warshel in the 1960s.[31] Other early efforts extended least squares optimization through use of *ab initio* calculations[32] and application to bulk phase crystal modeling.[33] Recently, force matching techniques have played a major role in development of both atomistic and coarse grained models.[34,35,36] ForceBalance[37,38,39] (Figure 1) extends this prior work in several directions, including the ability to use a larger and more diverse data set which includes experimental liquid phase measurements and *ab initio* calculations. The overall objective function is expressed as a weighted sum of squared residuals over the experimental and theoretical target data sets. Recently, ForceBalance has been used to derive two new, rigid, fixed partial charge water models, TIP3P-FB and TIP4P-FB.[39]

In the present work, we derive a revised set of parameters for the AMOEBA water model using the ForceBalance methodology. The new model, to be referred to as AMOEBA14, represents a significant improvement over the original 2003 AMOEBA water parameterization[40] (herein referred to as AMOEBA03). The AMOEBA14 model provides a significant improvement in the ability to predict experimental and *ab initio* data, particularly for a number of liquid properties across a range of temperatures. In addition, we provide some initial results to show the new model is capable of yielding acceptable results of ion-water energetics, which holds promise of compatibility of AMOEBA14 water with the previously determined AMOEBA force fields for organic molecules[41] and for proteins.[42]

METHODOLOGY

AMOEBA Model

The atomic multipole optimized energetics for biomolecular applications (AMOEBA)[40] water model in this work has the functional form:

$$E = E_{bond} + E_{angle} + E_{b\theta} + E_{vdW} + E_{ele}^{perm} + E_{ele}^{ind} \quad (1)$$

The first three terms describe the short-range interactions, including bond stretching, angle bending, and the Urey-Bradley bond-angle cross term. The bond stretching parameters includes anharmonicity up to second order deviations from the ideal bond length

$$E_{bond} = K_b(b - b_0)^2 \left[1 - 2.55(b - b_0) - 3.793125(b - b_0)^2 \right] \quad (2)$$

and the angle bending function includes up to fourth order deviations from the ideal angle

$$E_{angle} = K_\theta(\theta - \theta_0)^2 \left[1 - 0.014(\theta - \theta_0) + \left(5.6 \times 10^{-5} \right)(\theta - \theta_0)^2 - \left(7.0 \times 10^{-7} \right)(\theta - \theta_0)^3 + \left(2.2 \times 10^{-8} \right)(\theta - \theta_0)^4 \right] \quad (3)$$

The Urey-Bradley parameters follow a harmonic functional form

$$U_{UB} = K_\ell(\ell - \ell_0)^2 \quad (4)$$

The remaining three terms in Equation 1 describe the nonbonded van der Waals (vdW) interactions and the electrostatic contributions from both permanent and induced dipoles. The vdW term follows a Halgren buffered 14-7 potential to model the pairwise additive interactions for dispersion at long-range and exchange repulsion at short-range[43],

$$E_{ij}^{buff} = \varepsilon_{ij} \left(\frac{1+\delta}{\rho_{ij}+\delta} \right)^{n-m} \left(\frac{1+\gamma}{\rho_{ij}^m + \gamma} - 2 \right) \quad (5)$$

and which is less steep than the Lennard-Jones functional form. The nonbonded van der Waals (vdW) parameters we use are n=14, m=7, δ=0.07, γ=0.12, the well depth ε_{ij}, and $\rho_{ij} = \frac{R_{ij}}{R_{ij}^0}$ where R_{ij} is the i-j separation and R_{ij}^0 is the minimum energy distance. Van der Waals parameters are included for both oxygen and hydrogen atoms. The hydrogen reduction factor moves the hydrogen vdW center toward the oxygen along the bond length. For example, a reduction factor of 0.80 would move the hydrogen vdW center 20% of the bond length toward the oxygen.

The permanent electrostatic term includes the atomic monopole, dipole and quadrupole moments for each atom center. The polarization effects within the AMOEBA water model include mutual polarization by mutual induction of the dipoles for each atom. The non-additive definition of the model translates to each atom within the water molecule being a polarizable site and experiencing the mutual polarization. As a consequence of the non-additive mutual definition of the AMOEBA model, a polarization catastrophe would arise if a damping scheme were not introduced; therefore, the polarization parameters for the

AMOEBA water model include the polarizability of oxygen and hydrogen and a damping factor related to Thole's description of damping.[44] The distribution of the charge (ρ) in AMOEBA has the functional form

$$\rho = \frac{3\alpha}{4\pi} exp\left(-au^3\right) \quad (6)$$

with a representing the damping parameter[44] controlling how strongly the charge distribution is smeared and u is the distance relating the polarizabilities of atomic sites i and j [$u = R_{ij}/(\alpha_i\alpha_j)^{1/6}$].

For the mutual model, the induced dipole is calculated at each atomic site via

$$\mu_{i,\alpha}^{induc} = \alpha_i E_{i,\alpha} = \alpha_i \left(\sum_{\{j\}} T_\alpha^{ij} M_j + \sum_{\{j\}} T_{\alpha\beta}^{ij'} \mu_{j',\beta}^{induc}\right) \text{ with } \alpha, \beta = 1, 2, 3 \quad (7)$$

where α_i is the atom polarizability, $E_{i,\alpha a}$ represents the electric fields generated by permanent multipoles and induced, $M_j = [q_j, \mu_{j1}, \mu_{j2}, \mu_{j3}, \ldots]^T$ includes the permanent multipole components and $T_\alpha^{ij} = [T_\alpha, T_{\alpha 1}, T_{\alpha 2}, T_{\alpha 3}, \ldots]$ represents the matrix for the interaction of sites i and j where $T_\alpha = \nabla_\alpha T = -\frac{R_\alpha}{R^3}$ and $T_{\alpha\beta} = \nabla_\alpha T_\beta$. The summations are carried out over two sets: {j}, all atom sites outside the molecule containing atom site i, and {j'}, all atom sites other than i. The function for the induced dipoles self-consistently reduces to

$$\mu_{i,\alpha}^{induc}(n+1) = \mu_{i,\alpha}^{induc}(n) + \alpha_i \left(\sum_{\{j\}} T_{\alpha\beta}^{ij'} \mu_{j',\beta}^{induc}(n)\right) \text{ with } n = 0, 1, 2, \ldots \quad (8)$$

From this solution, the first term in Equation 8 represents the direct induced dipole for atom i as a result of the electric field generated from the permanent multipoles from neighboring molecules. The second term represents the mutual induced dipole resulting from induced dipoles induced on all other atom sites. The mutual induction calculation is iterated until the induced dipoles are no longer induced by dipoles on all other sites with a tolerance set to 10^{-5} D.

For the reparameterization of the AMOEBA functional form, there were 21 tunable parameters included in the optimization: the vdW radius (R) and potential well depth (ε) for oxygen and hydrogen, reduction factor for hydrogen, bond-stretching force constant (Kb) and length (b), angle-bending force constant (K_θ) and magnitude (θ), Urey-Bradley force constant ($K_/$) and length (/), charge for hydrogen and oxygen, multipoles (dipole, quadrupole) for hydrogen and oxygen, the polarizability for hydrogen and oxygen, and the Thole polarization damping factor.

Simulation Protocol

Initial cycles of ForceBalance used a cubic box with an initial side length 18.65 Å and containing 216 water molecules. Molecular dynamics in the NPT ensemble was performed

via a Martyna-Tuckerman-Klein integrator incorporating a Nose-Hoover thermostat and barostat.[45] Final liquid parameter optimization cycles were also done on 216 waters. Each final simulation was run for four nanoseconds following 400 picoseconds of equilibration. The simulations for the final parameterization employed Langevin dynamics with a multiple timestep velocity Verlet integrator with the Langevin friction force and random force. The Langevin dynamics used a friction coefficient of 1.0 picoseconds^{-1}. These final simulations used a Monte Carlo barostat with a trial frequency of 1 box size change per 25 MD steps. All dynamics simulations were performed with either the TINKER[46] or OpenMM[47] modeling software packages. Properties, including the self-diffusion constant, viscosity, dielectric constant, enthalpy of vaporization, heat capacity, isothermal compressibility and 2nd virial coefficient, were computed by the same methods used for the earlier AMOEBA03 water model.[40]

Calibration Data

The data utilized for fitting the parameters was composed of a combination of experimentally-determined condensed phase properties as well as robust *ab initio*-derived properties. The condensed phase properties considered were the density, enthalpy of vaporization, isothermal compressibility, isobaric heat capacity, thermal expansion coefficient, and dielectric constant. The temperature and pressure combinations were: 1 atmosphere at temperatures ranging from 249 K to 373 K (32 total), and 298 K at pressures from 1 kilobar to 8 kilobar (8 total). The complete lists of temperatures, pressures, and values for each experimental property are included in the Supplemental Information.

The *ab initio* reference data included properties for systems ranging in size from the monomer to clusters of 22 water molecules. For the monomer, the charge, dipole, quadrupoles, polarizability, vibrations, and geometry were considered. The *ab initio* interaction energies and ground state geometries for the ground state dimer, Smith dimer set (10 total),[48] trimer, tetramer, pentamer, eight hexamers,[49] two octamers,[50] five 11-mers,[51] five 16-mers, two 17-mers, and four 20-mers[52,53] were utilized for calibration. In previous work,[54] over 42000 clusters (ranging from two to 22 water molecules) geometries were obtained from AMOEBA simulations of liquid water for temperatures ranging from 249 K to 373 K. Energies and gradients for the clusters were determined via RI-MP2[55,56]/heavy-aug-cc-pVTZ[57] as implemented in Q-Chem 4.0.[58] This large compilation of theoretical data was included in the fitting of the AMOEBA water parameters.

ForceBalance

The AMOEBA03 water model was parameterized by hand to fit results from *ab initio* calculations on gas phase clusters,[40] and temperature and pressure dependent bulk phase properties.[59] Here we apply ForceBalance, an automatic optimization method, to parameterize a revised AMOEBA14 model using the expanded data set described in the last section. ForceBalance has previously been applied to the development of a direct polarization variant of AMOEBA, labeled iAMOEBA, which omits the self-consistent calculation of polarization interactions.[54] One of the goals for iAMOEBA was to accurately describe bulk phase properties; therefore, the condensed phase properties, *e.g.* density, were given a greater weight than gas phase properties, such as cluster interaction energies.

Ideally, the mutual AMOEBA model should be applicable across all system sizes and phases as well. To reflect this goal for the mutual polarization model, each property in the calibration set was initially given an equal weight. This is in contrast to the previous direct polarization water model, where the condensed phase experimental data was weighted more heavily than the gas phase cluster data.

The enthalpy of vaporization measures the water-water interaction strength, while the related property of the density reflects the hydrogen-bonded network structure, both of which have significant temperature (and pressure) dependence. If the enthalpy value is too large or its change with temperature is too steep, then the attraction between the water molecules is too great and the heat capacity would be too high. This would be problematic for not only the homogeneous water system, but in heterogeneous systems where the water-water, water-solute, and solute-solute interactions need to be balanced. For example, a temperature of maximum density (TMD) of a model that is very different than the experimental TMD would likely change the trends in hydrophobic hydration with temperature, since the entropic penalty for cavity formation in the liquid by definition changes with temperature. Therefore, the weighting of the condensed phase properties was adjusted to increase the weights of the enthalpy of vaporization and density in relation to the other condensed phase properties. The whole set of condensed phase properties maintained equal weighting with the gas phase data, but the individual condensed phase properties were assigned different weights with respect to each other.

ForceBalance supports many different optimization algorithms, and the calculation in this work was carried out using the trust-radius Newton-Raphson (or Levenberg-Marquardt[60,61]) algorithm with an adaptive trust radius.[62,63] This algorithm requires the first and second derivatives of the objective function in the parameter space, which we derive from the first derivatives of the simulated properties using the Gauss-Newton approximation.

A major challenge in force field parameterization is the significant statistical noise in the objective function from the sampling of properties to be matched to experiment. The parametric derivatives are challenging to evaluate because numerical differentiation requires running multiple simulations and evaluating small differences between statistically noisy estimates. ForceBalance uses thermodynamic fluctuation formulas to calculate accurate parametric derivatives of simulated properties without running expensive multiple simulations.[38, 64] For instance, the ensemble average of a generic observable A that does not depend explicitly on the force field parameters (for example, the density or an order parameter) can be expressed as follows:

$$\begin{aligned} \langle A \rangle_\lambda &= \tfrac{1}{Q(\lambda)} \int A(\mathbf{r}, V) \, exp\left(-\beta \left(E(\mathbf{r}, V; \lambda) + PV\right)\right) d\mathbf{r} \, dV \\ Q(\lambda) &= \int exp\left(-\beta \left(E(\mathbf{r}, V; \lambda)\right) + PV\right) d\mathbf{r} \, dV \end{aligned} \tag{9}$$

where A is the observable, $\mathbf{r}$ a given molecular configuration in a periodic simulation cell, l the force field parameter, E the potential energy, $\beta \equiv (k_B T)^{-1}$ the inverse temperature, k_B the Boltzmann constant, T the temperature, P the pressure, V the volume, Q the isothermal-isobaric partition function, and the angle brackets with a l subscript represent an ensemble average in the thermodynamic ensemble of the force field parameterized by l. In practice,

this integral is evaluated numerically using molecular dynamics or Monte Carlo simulation in the NPT ensemble.

Since the expression for *A* depends on *l* only through the potential energy *E*, we can differentiate Equation 9 analytically:

$$
\begin{aligned}
\frac{d}{d\lambda}\langle A\rangle_\lambda &= \frac{1}{Q(\lambda)}\int A(\mathbf{r},V)\,exp\left(-\beta\left(E(\mathbf{r},V;\lambda)+PV\right)\right)\left(-\beta\frac{dE(\mathbf{r},V)}{d\lambda}\right)d\mathbf{r}\,dV \\
&\quad -\frac{1}{Q(\lambda)^2}\frac{dQ}{d\lambda}\int A(\mathbf{r},V)\,exp\left(-\beta\left(E(\mathbf{r},V;\lambda)+PV\right)\right)d\mathbf{r}\,dV \\
&= -\beta\left(\left\langle A\frac{dE}{d\lambda}\right\rangle_\lambda - \langle A\rangle_\lambda\left\langle\frac{dE}{d\lambda}\right\rangle_\lambda\right)
\end{aligned}
\tag{10}
$$

The potential energy derivative $\left\langle\dfrac{dE}{d\lambda}\right\rangle$ is evaluated by numerically differentiating the potential energies at the sampled structures. Equation 10 provides a way to evaluate the parametric derivative of thermodynamic properties without running additional sampling simulations, though the derivative of any observable always manifests as a higher order correlation function and has a larger statistical error than the observable itself. This equation may be directly applied to obtain derivatives of ensemble-averaged observables with implicit parametric dependence through the thermodynamic ensemble, such as the density ρ. Equation 10 is easily extensible to obtain derivatives of observables with explicit parameter dependence, such as the enthalpy; derivatives for higher-order thermodynamic response properties such as the dielectric constant are obtained using the chain rule.[54] We omit the calculation of second parametric derivatives for reasons of computational cost and statistical noise, relying instead on the least-squares form of the objective function and the Gauss-Newton approximation to obtain the Hessian.

In order to maximize the efficiency of simulating properties, ForceBalance interfaces with several powerful and complementary technologies. ForceBalance includes interfaces to AMOEBA via the TINKER[46] modeling software and via OpenMM 6.1,[47] a graphics processing unit (GPU)-accelerated MD engine. The Work Queue library[65] allows ForceBalance to parallelize multiple simulations across compute nodes in different physical locations. ForceBalance analyzes the data from finished simulations using the multistate Bennett acceptance ratio estimator (MBAR)[66] which allows multiple simulations at different thermodynamic phase points to statistically contribute to one another. All of these software packages and methods are freely available on the Web.

The problem of overfitting is treated by regularization via a penalty function, which corresponds to imposing a *prior* distribution of parameter probabilities in a Bayesian interpretation. The prior widths reflect the expected variations of the parameters during the optimization, which may be chosen heuristically or sampled over in an empirical Bayes approach. Our optimization was regularized using a Gaussian prior specified in Table 1, corresponding to a parabolic penalty function in parameter space centered at the original AMOEBA parameter values with the chosen force constants. Since the various parameters have different physical meanings (*e.g.* vdW well depth, O-H bond length), each parameter type was assigned its own prior width.

We ran the optimization until fluctuations from numerical noise prevented further improvement. The calculation converged to within the statistical error after about 10 nonlinear iterations, though we performed several optimizations with different choices of weights for the reference data and prior widths before arriving at the final answer.

RESULTS AND DISCUSSION

AMOEBA14 Water Parameters

The parameters for the new AMOEBA14 water model, the AMOEBA03 model, and the Gaussian prior widths included in the ForceBalance optimization are reported in Table 1. The prior widths are proportional to the inverse-squared strength of the harmonic penalty for each parameter and reflect the parameter's intrinsic size and expected variability. It should be noted, the bond force constant, angle force constant, and the Urey-Bradley parameters for AMOEBA03 were modified in 2013 when it was observed the original parameters incorrectly predicted the order of the vibrational frequencies; therefore, the comparison we are making for intramolecular parameters is to those revised parameters. Table 1 shows that the intramolecular parameters for the AMOEBA model remained essentially unchanged from 2003 to 2014.

The damping value of 0.39 was kept fixed during the AMOEBA14 model optimization since the value in the 2003 model was set based on water cluster energies, and this damping value has been tested and employed for the majority of atom classes within the AMOEBA model. For the AMOEBA03 water model, the polarizability parameters for oxygen and hydrogen were those proposed by Thole. While the polarizability values were allowed to fluctuate during the ForceBalance optimization of AMOEBA14, they do not deviate significantly from the AMOEBA03 model.

Repulsion-dispersion parameters (vdW radius and well-depth) were assigned to both the oxygen and hydrogen atom centers. AMOEBA14 has a larger vdW radius and well-depth for oxygen and a smaller vdW radius and well-depth for hydrogen compared to AMOEBA03. The newly proposed reduction factor for hydrogen shifts the hydrogen vdW center toward oxygen by approximately 20% of the O-H bond length. The parameter optimization approached a point of zeroing out the hydrogen vdW site and reducing the model to one repulsion-dispersion site on oxygen, but the final set of parameters include both atoms and the description of the water oxygen is consistent with the description of oxygen in other organic molecules for the AMOEBA model.

The AMOEBA14 water model increases the charge of the oxygen and decreases the charge of the hydrogen in comparison to the AMOEBA03 model. The z-component of the oxygen dipole is less than AMOEBA03 and the x- and z-components of the hydrogen dipole are greater. There are substantial deviations for both the oxygen and hydrogen quadrupole parameters in relation to the AMOEBA03 model. The xx-component of the quadrupole moment tensor decreases by approximately the same magnitude by which the yy-component of the quadrupole increases for oxygen. An increase of the same scale is observed for the xx- and yy-components of the quadrupole moment tensor for hydrogen, but there is a sign change for these hydrogen quadrupole parameters. These changes in the non-bonded

interactions reflect improvements in the gas phase and condensed phase properties of water described in the next sections.

AMOEBA14 Fitted Gas Phase Water Properties

Table 2 provides the multipole properties predicted by the AMOEBA14 and AMOEBA03 water models. The AMOEBA14 water parameters predict the dipole of a gas phase water monomer to be 1.808 Debye in comparison to the experimental value of 1.855 Debye. The changes in the atomic quadrupole parameters improve the molecular *xx*-quadrupole moment compared to experiment, while the *yy*- and *zz*-quadrupole moments are nearly unchanged in comparison to the AMOEBA03 model.

As in the original AMOEBA model, the ideal bond angle is larger than the experimental and ab initio values. The three vibrational frequencies of the water monomer are predicted to within 0.3 cm^{-1} and the ordering of the modes is in agreement with experiment. In Table 3 the AMOEBA water dimer equilibrium structure and interaction energy are compared to experiment and *ab initio* results. For the equilibrium dimer minimum, the AMOEBA14 model is in somewhat poorer agreement with *ab initio* values than the earlier AMOEBA03 model. However, averaged over a series of low energy dimer configurations, the AMOEBA14 is as good as or superior to AMOEBA03. As previously noted, ten *ab initio* dimer interaction energies and geometries were including in the fitting of the model parameters. The root mean squared deviations (RMSDs) for the monomer and dimer geometries were 0.017 and 0.057 Å, respectively.

The interaction energies for water clusters, ranging from dimers to clusters of 20 water molecules (see Table 4), were analyzed with the AMOEBA water model. The geometries of the clusters were optimized and the interaction energy determined via AMOEBA. The cluster results are compiled in Table 4. The mean absolute deviation (MAD) for the interaction energy of the smaller clusters (2-8 water molecules) is 0.39 kcal/mol, considered to be within chemical accuracy (*i.e.*, within 1 kcal/mol of experiment). Specific results for the hexamers are shown in Figure 2. The larger clusters (11- to 20-mers) have an MAD of 7.97 kcal/mol for the interaction energy prediction. The discrepancy between the accuracy levels of the AMOEBA water model for the small and large clusters is interesting and would suggest the error of AMOEBA with respect to system size could be systematic. To examine this possibility, the MADs of each of the condensed phase properties (discussed further below) was tabulated in Table 5, and the errors were of the same magnitude as the small clusters.

In the analysis of the 42000 clusters (~2400 clusters of *n* water molecules, *n*=2-22), the potential energies, gradients, net forces, and torques were computed with AMOEBA14 and compared to the *ab initio* reference data. As a specific example of the results, the root mean squared (RMS) errors for the cluster of 18-mers were 7.8 kJ/mol (10%) for energy, 33.8 kJ/mol/Å (42%) for the gradient, 9.9 kJ/mol/Å (30%) for the net force, and 6.3 kJ/mol/rad (25%) for the torque. The standard deviations for the reference data were 29.2 kJ/mol, 83 kJ/mol/Å, 29 kJ/mol/Å, and 20 kJ/mol/rad, for the energies, gradients, forces, and torques, respectively. Over all of the cluster sizes, the AMOEBA14 model predicted the potential energies to, on average, within 15% of the reference. This accuracy level is surprising when

the weighting of the reference data is considered. The bulk clusters were assigned the smallest weights, *i.e.*, fitting the energies and gradients were the lowest priority in the parameter optimization. The robustness of the AMOEBA14 model in comparison to *ab initio* cluster reference data reaffirms the utility of the model for both gas and bulk phase properties.

The second virial coefficient of water computed with an empirical potential is a sensitive measure of the accuracy of the Boltzmann-weighted dimer potential energy surface. Following Millot, *et al.*, we computed the classical virial coefficient, as well as first-order translational and rotational quantum corrections.[67] Some workers have argued that the quantum corrections are unnecessary as they are implicitly incorporated into empirical water potentials.[68] Others have emphasized the importance of higher-order corrections and experimental error, especially at temperatures below about 325 K.[69] Figure 3 shows both the classical and first-order corrected second virial coefficients for the AMOEBA03 and AMOEBA14 models. The two models exhibit very similar behavior, and in both cases the uncorrected coefficients are in excellent agreement with experiment. Nonpolarized models intended for use in the bulk phase simulation tend to lie below the experimental second virial curve, especially at low temperature. The iAMOEBA model (not shown) is also somewhat underpolarized, and also yields second virial coefficients that are too negative.

In previous work,[28] the dependence of the density maximum on the water geometry was explored. The 2003 model adopted an equilibrium angle of 108.5° in the gas phase ("correct" value per *ab initio:* 104.5°) in order to achieve an average angle of 105.3° in the condensed phase and be in near agreement with experiment at room temperature. With the re-optimized AMOEBA parameters, the equilibrium gas phase angle is 107.8° and the condense phase angle is 105.1°. The average AMOEBA14 H-O-H angle slightly increases (104.9° to 105.4°) as the temperature increases from 249 K to 373 K. While previous theoretical estimates concluded the liquid water should see the angle contract with increasing temperature,[70] experimental data has reported no relation between angle magnitude and temperature.[71]

AMOEBA14 Fitted Condensed Phase Water Properties

In the parameterization of the initial AMOEBA03 water model, only the density and heat of vaporization at room temperature were considered. Within the fitting of the current model, six condensed phase properties were considered at a range of temperatures (249 K to 373 K) and pressures (1 atm to 8 kilobar). For AMOEBA14, the enthalpy of vaporization and density trends with temperature were the focal points in the fit and were given a greater weight in the optimization. All of the thermodynamic data and their trends with respect to temperature are shown in Figures 2-5, while tables with the raw numbers are included in the Supplemental Information.

Since AMOEBA03 was specifically fit to the enthalpy of vaporization and the density at room temperature, the initial model agrees with the corresponding experimental values to within statistical error. However, the linear temperature dependence of the enthalpy of vaporization only intersects with the experiment at room temperature. With the AMOEBA14 water model, the enthalpy of vaporization at room temperature differs by only

0.49 kcal/mol over the temperature range examined, and the mean absolute deviation (MAD) of the model was 0.43 kcal/mol compared to 0.65 for AMOEBA03 (Figure 4). The experimental maximum density of 999.972 kg/m^3 occurs at 277.15 K and 1.0 atm of pressure. The temperature of maximum density as predicted by the AMOEBA03 model is shifted to higher temperatures by nearly 15 K, and the curve of the temperature dependence is slightly narrower. The new AMOEBA14 water parameters yield a temperature of maximum density in quantitative agreement with experiment and the shape of the curve is in qualitative agreement with experiment. (Figure 5).

The AMOEBA14 results for the thermodynamic fluctuation properties (heat capacity, isothermal compressibility, and thermal expansion coefficient) are shown in Figures 6-9. Since the temperature dependence of the predicted enthalpy of vaporization has a slightly greater slope than experiment (Figure 4), the calculated heat capacity for AMOEBA14 is greater than experiment by, on average, 2.28 cal/mol/K. AMOEBA14 improves upon the AMOEBA03 model, whose enthalpy of vaporization temperature dependence is much steeper, resulting in much higher heat capacity values. The discrepancy between the AMOEBA14 calculated and experimental heat capacity is due to the approximations within our classical, flexible model, and previous work has estimated the accuracy of the heat capacity determined by AMOEBA to be ±5 cal/mol/K.[28] While an overestimation of the heat capacity means an overestimation of the entropy fluctuations, what matters more is that the temperature onset of anomalous fluctuations (i.e. above the normal background) is better described by the AMOEBA14 model relative to AMOEBA03 (Figure 6).[72]

The AMOEBA14 model also shows a drastic improvement in the quantitative value of the isothermal compressibility in comparison to the 2003 model, which overestimates the compressibility by ~30% at ambient conditions. Again, the more important point is that the temperature trends are correct for AMOEBA14, with a compressibility minimum very near the 319K value seen experimentally (Figure 7). AMOEBA14 not surprisingly shows the transition from positive to negative thermal expansion coefficient at the same temperature as experiment, which is to be expected given that the TMDs are the same (Figure 8).

Finally, Figure 9 shows the temperature dependence of the dielectric constant, which is in excellent agreement with experiment, and also agrees well with the AMOEBA03 value of ~80 at room temperature. The excellent reproduction of the dielectric constant for the AMOEBA14 model is due to a good balance within the electrostatic model. Carnie and Patey showed the dipolar correlations are suppressed when the quadrupole interactions increase, thereby decreasing the dielectric constant of the liquid.[73] It has been noted[74] that since the dielectric response arises from both the magnitude as well as the fluctuations of the water dipole, by definition, a good dielectric constant can be achieved by a model with either small dipoles with large fluctuations (corresponding to small quadrupoles < ~1.8 D-Å) or large dipoles with small fluctuations (large quadrupoles > ~2.5 D-Å). It appears, therefore, that the polarization of the AMOEBA models give rise to dipoles that are large enough to overcome the quadrupolar quenching in achieving its excellent dielectric properties.

AMOEBA14 Validation

Radial Distribution Function—The radial distribution functions (RDFs) can be derived from X-ray scattering and neutron diffraction[75,76] and provide information about the structure of liquid water. Figure 10 shows the oxygen-oxygen RDF curve of the AMOEBA03, AMOEBA14 and iAMOEBA models when compared against the ALS[77] and more recent APS[78] experimental estimates of the real space structure derived from the intensity data. The gOH(r) and gHH(r) curves are included in the Supplemental Information. The AMOEBA14 model is in overall good agreement with experiment for the three distributions. The height of the first peak in gOO(r) is approximately 0.4 and 0.6 greater than the ALS and APS X-ray data, respectively, but the location of the peak is at the same oxygen-oxygen distance as experiment. The first and second troughs, as well as the second peak, of the gOO(r) nearly overlap the experimental curve, with deviations of less than 0.1%. A similar level of agreement is seen between the AMOEBA models and experiment for the gOH(r) and gHH(r), and as an effective potential it probably captures, imperfectly, any nuclear quantum effects.

Assuming a model for the condensed phase water electron density based on modified atomic form factors (MAFFs)[77], we can Fourier transform the radial distribution functions to derive a simulated intensity curve to compare against the ALS[71] and APS[78] intensity data (Figure 11). Since the RDFs were not included in the calibration data, we performed three optimizations with different molecular polarizability targets (1.35, 1.41 and 1.47 Å^3) to determine its effect on water structure. The lower bound is based on an earlier *ab initio* calculation that suggested a reduction in the molecular polarizability in going from gas phase (1.47 Å^3) to the condensed phase (1.35 Å^3).[80] More recent work has evaluated the molecular polarizability in the liquid using a different method, and determined that it was not significantly different from the gas phase value.[81] It is evident from Figure 11 that modifying, within reason, the polarizability, produced no qualitative difference in the RDFs, although other properties may be sensitive to other water properties, although we do not investigate them here. Overall the AMOEBA model intensities fall outside the differences between the ALS and APS experiments, which is likely a result of the larger first peak in the gOO(r) compared to experimental estimates.

Electrostatic Potential—The general protocol in the development of novel AMOEBA parameters typically optimizes the atomic multipole parameters by fitting to the molecular electrostatic potential generated via a gas phase *ab initio* molecular orbital calculation.[41] As detailed above, the AMOEBA14 water multipole parameters were allowed to fluctuate in conjunction with the remaining parameters and the monomer electrostatic potential map was not included in the fitting. The TINKER POTENTIAL program was used to compare the electrostatic potential for a single water molecule on a dense, uniform grid of points in a band 1.0 to 2.05 Å from the vdw surface. The average magnitude for the electrostatic potential from an MP2/aug-cc-pVQZ calculation was 6.6851 kcal/mol/e- and the deviations for AMOEBA03 and AMOEBA14 werefound to be −0.0499 and −0.0584. While the AMOEBA14 model was not fit to the *ab initio* electrostatic potential, the model is clearly effective for gas phase calculations outside of the calibration data.

Transport and Surface Tension Properties at Room Temperature—The viscosity, self-diffusion constant, and the surface tension at room temperature, were computed for the AMOEBA14 model. Viscosity was computed via the Einstein-Helfand relation and using the off-diagonal components of the pressure tensor. The viscosity of AMOEBA14 is 0.900 centipoise (cP) and is in nearly perfect agreement with the experimental measurement of 0.896 cP at 298 K.[82] Self-diffusion was computed via the Einstein equation via average motion over all molecules across a full MD simulation. The standard self-diffusion coefficient as determined from an NPT simulation with 216 molecules in a periodic box is 1.99×10^{-5} cm^2/s, which underestimates the experimental self-diffusion coefficient of 2.29×10^{-5} cm^2/s. Yeh and Hummer have suggested an analytical system-size correction for diffusion coefficients computed via periodic MD simulation.[83] Application of their correction increases the AMOEBA14 value to 2.36×10^{-5} cm^2/s. The surface tension computed via averaging over the diagonal elements of the pressure tensor is $\gamma = 69.21$ N/m, and deviates less than 0.5% from the corresponding experimental value determined at 298 K.[84] All of these properties are summarized in Table 6.

Ion-Water Interactions—It is important to validate the AMOEBA14 water model for not only a homogeneous system, but also a heterogeneous system. The ion-water interaction was examined for the gas phase dimer system and the ion hydration free energy. The ions considered were the sodium cation (r=2.85, ε=0.15, α=0.12) and chloride anion (r=4.20, ε=0.5, α=4.0). Ion hydration free energies were computed via the orthogonal space random walk (OSRW) method.[85] The binding energies and equilibrium distance for the ion-water dimer and the ion hydration free energies are reported in Table 6. The AMOEBA14 model predictions for the ion-water dimer interaction energies are within 0.5 kcal/mol of experiment, while the ion hydration free energies are slightly overestimated for both the anion and the cation. Since water-ion intermolecular interactions are large and involve significant polarization, it is encouraging that the ion parameters required only minor adjustment from the 2003 values[28] for use with AMOEBA14. While much further testing is necessary, this holds promise that AMOEBA parameters for other systems will retain compatibility with the new AMOEBA14 water model.

CONCLUSION

The inclusion of polarizability makes the AMOEBA model preferable over other fixed-charge water models when characterizing water at different state points, for asymmetric environments, and for better transferability. With the advances made in computational modeling over the past decade, the AMOEBA water model was revisited in order to calibrate the parameters against a large, diverse data set. The new AMOEBA water model improves in accuracy over the original model for the prediction of bulk properties over large temperature and pressure ranges, in addition to maintaining reliability for gas phase property determination. By utilizing the ForceBalance methodology to optimize the AMOEBA model, nearly two dozen parameters could be systematically fit to a data set of *ab initio* calculations and experimental measurements.

The new AMOEBA water model is an improvement over the previous model, since a range of temperatures and pressures, as well as more gas phase and bulk properties, were included

in the fitting of the parameters. For the six condensed phase properties in the calibration data set, AMOEBA14 qualitatively matches the experimental curves over the temperature range and the deviations from experiment are generally within a reasonable error margin. The current model exactly matches the experimental temperature of maximum density and the enthalpy of vaporization at room temperature differs by less than 0.5 kcal/mol, with a mean absolute deviation of 0.43 kcal/mol over the temperature range studied. The improvement observed for the bulk phase prediction of the AMOEBA14 model does not come at the expense of the accuracy of the model for gas phase property determination. The AMOEBA14 model has a similar accuracy level as the AMOEBA03 model for the interaction energy of gas phase cluster ranging from dimers to 20-mers. The integrity of the new model parameters holds for properties not included in the calibration data set, as evidenced by the good agreement observed between the experimental radial distribution functions for oxygen-oxygen, oxygen-hydrogen, and hydrogen-hydrogen and those obtained via AMOEBA14.

The development of the new AMOEBA14 parameters is significant for modeling systems solvated in water, where the balance of solvent-solvent, solvent-solute, and solute-solute interactions is crucial for determining solute behavior. Within this work we have demonstrated the accuracy of the AMOEBA14 model for a heterogeneous system, specifically the calculation of ion hydration free energies. Future applications of the model, for example, determining ligand binding affinities, will benefit from the improved definition of the AMOEBA water parameters.

It should be noted, most current generation water models are missing an explicit term to account for charge penetration effects. Such a term is needed to correct for the use of point charges, or point multipoles in the case of AMOEBA, restricted to nuclear positions. A variety of empirical and semi-empirical damping functions have been proposed to treat penetration in the context of both molecular mechanics,[86,87,88] including the AMOEBA benzene dimer,[89] and QM/MM calculations.[90,91] We plan to explore how charge penetration effects within the AMOEBA model impact the water parameterization. For example, the preliminary indication is inclusion of charge penetration reduces the largest differences between *ab initio* and AMOEBA dimer energies (see Table 4).

With the improved accuracy of the AMOEBA water model for bulk phase property prediction, we recommend the implementation of our revised parameters for future studies employing a polarizable water model. The model is proven to be transferable between gas phase and bulk phase, as well as in homogeneous and heterogeneous systems.

Supplementary Material

Refer to Web version on PubMed Central for supplementary material.

Acknowledgements

REFERENCES

1. Bernal JD, Fowler RH. A Theory of Water and Ionic Solution, with Particular Reference to Hydrogen and Hydroxyl Ions. J. Chem. Phys. 1933; 1:515–548.

2. Jorgensen WL, Chandrasekhar J, Madura JD, Impey RW, Klein ML. Comparison of Simple Potential Functions for Simulating Liquid Water. J. Chem. Phys. 1983; 79:926–935.

3. Rahman A, Stillinger FH. Molecular Dynamics Study of Liquid Water. J. Chem. Phys. 1971; 55:3336–3359.

4. Stillinger FH, Rahman A. Improved Simulation of Liquid Water by Moleculer Dynamics. J. Chem. Phys. 1974; 60:1545–1557.

5. Berendsen, HJC.; Postma, JPM.; van Gunsteren, WF.; Hermans, J. Interaction Models for Water in Relation to Protein Hydration. In: Pullman, B., editor. Intermodular Forces. Reidel; Dordrecht, Netherlands: 1981. p. 331-342.

6. Head-Gordon T, Stillinger FH. An Orientational Perturbation Theory for Pure Liquid Water. J. Chem. Phys. 1992; 98:3313–3327.

7. Mahoney MW, Jorgensen WL. A Five-Site Model for Liquid Water and the Reproduction of the Density Anomaly by Rigid, Nonpolarizable Potential Functions. J. Chem. Phys. 2000; 112:8910–8922.

8. Berendsen HJC, Grigera JR, Straatsma TP. The Missing Term in Effective Pair Potentials. J. Phys. Chem. 1987; 91:6269–6271.

9. Horn HW, Swope WC, Pitera JW, Madura JD, Dick TJ, Hura GL, Head-Gordon T. Development of an Improved Four-Site Water Model for Biomolecular Simulations: TIP4P-Ew. J. Chem. Phys. 2004; 120:9665–9678. [PubMed: 15267980]

10. Levitt M, Hirshberg M, Sharon R, Laidig KE, Daggett V. Claibration and Testing of a Water Model for Simulation of the Molecular Dynamics of Proteins and Nucleic Acids in Solution. J. Phys. Chem. B. 1997; 101:5051–5061.

11. Matsuoka O, Clementi E, Yoshimine M. CI Study of the Water Dimer Potential Surface. J. Chem. Phys. 1976; 64:1351–1361.

12. Vesely FJ. N-Particle Dynamics of Polarizable Stockmayer-type Molecules. J. Comput. Phys. 1977; 24:361–371.

13. Barnes P, Finney JL, Nicholas JD, Quinn JE. Cooperative Effects in Simulated Water. Nature. 1979; 282:459–464.

14. Warshel A, Kuwajima S. Incorporating Electric Polarizabilities in Water-Water Interaction Potentials. J. Phys. Chem. 1990; 94:460–466.

15. Sprik M, Klein ML. A Polarizable Model for Water Using Distributed Charge Sites. J. Chem. Phys. 1988; 89:7556–7560.

16. Wallqvist A, Ahlstrom P, Karlstrom G. A New Intermolecular Energy Calculation Scheme: Applications to Potential Surface and Liquid Properties of Water. J. Phys. Chem. 1990; 94:1649–1656.

17. Caldwell J, Dang LX, Kollman PA. Implementation of Nonadditive Intermolecular Potentials by Use of Molecular Dynamics: Development of a Water-Water Potential and Water-Ion Cluster Interactions. J. Am. Chem. Soc. 1990; 112:9144–9147.

18. Dykstra CE. Structures and Vibrational Frequencies of Small Water Complexes from Electrical Molecular Mechanics. J. Chem. Phys. 1989; 91:6472–6476.

19. Fanourgakis GS, Xantheas SS. Development of Transferable Interaction Potentials for Water: V. Extension of the Flexible, Polarizable, Thole-Type Model Potential (TTM3-F, v.3.0) to Describe the Vibrational Spectra of Water Clusters and Liquid Water. J. Chem. Phys. 2008; 128:154519. [PubMed: 18433247]

20. Lamoureux G, Harder E, Vorobyov IV, Roux B, MacKerell AD. A Polarizable Model of Water for Molecular Dynamics Simulations of Biomolecules. Chem. Phys. Lett. 2006; 418:245–249.

21. Kumar R, Wang FF, Jenness GR, Jordan KD. A Second Generation Distributed Point Polarizable Water Model. J. Chem. Phys. 2010; 132:014309. [PubMed: 20078163]

22. Stillinger FH, Carl CW. Polarization Model for Water and its Ionic Dissociation Products. J. Chem. Phys. 1978; 69:1473–1484.

23. Halley JW, Rustad JR, Rahman A. A Polarizable, Dissociating Molecular Dynamics Model for Liquid Water. J. Chem. Phys. 1993; 98:4110–4119.

24. Carl CW. A Variable Charge Central Force Model of Water and its Ionic Dissociation Products. J. Chem. Phys. 1996; 104:7255–7260.

25. Williams DE. Representation of the Molecular Electrostatic Potential by Atomic Multipole and Bond Dipole Models. J. Comput. Chem. 1988; 9:745–763.

26. Bayly CI, Cieplak P, Cornell WD, Kollman PA. A Well-Behaved Electrostatic Potential Based Method Using Charge Restraints for Deriving Atomic Charges: The RESP Model. J. Phys. Chem. 1993; 97:10269–10280.

27. Mao AH, Pappu RV. Crystal Lattice Properties Fully Determine Short-Range Interaction Parameters for Alkali and Halide Ions. J. Chem. Phys. 2012; 137:064104. [PubMed: 22897252]

28. Grossfield A, Ren PY, Ponder JW. Ion Solvation Thermodynamics from Simulation with a Polarizable Force Field. J. Am. Chem. Soc. 2003; 125:15671–15682. [PubMed: 14664617]

29. Cerutti DS, Swope WC, Rice JE, Case DA. ff14ipq: A Self-Consistent Force Field for Condensed-Phase Simulations of Proteins. J. Chem. Theory Comput. 2014; 10:4515–4534. [PubMed: 25328495]

30. Nerenberg PS, Jo B, So C, Tripathy A, Head-Gordon T. Optimizing Solute-Water van der Waals Interactions to Reproduce Solvation Rree Energies. J. Phys. Chem. B. 2012; 116:4524–4534. [PubMed: 22443635]

31. Lifson S, Warshel A. Consistent Force Field for Calculations of Conformations, Vibrational Spectra, and Enthalpies of Cycloalkane and n-Alkane Molecules. J. Chem. Phys. 1968; 49:5116–5129.

32. Maple JR, Hwang MJ, Stockfisch TP, Dinur U, Waldman M, Ewig CS, Hagler AT. Derivation of Class-II Force Fields. 1. Methodology and Quantum Force Field for the Alkyl Functional Group and Alkane Molecules. J. Comput. Chem. 1994; 15:162–182.

33. Williams DE. Transferable Empirical Nonbonded Potential Functions. Topics Curr. Phys. 1981; 26:3–40.

34. Ercolessi F, Adams JB. Interatomic Potentials from 1st-Principles Calculations-The Force-Matching Method. Europhys. Lett. 1994; 26:583–588.

35. Izvekov S, Parrinello M, Burnham CJ, Voth GA. Effective Force Fields for Condensed Phase Systems from ab Initio Molecular Dynamics Simulation: A New Method for Force-Matching. J. Chem. Phys. 2004; 120:10896–10913. [PubMed: 15268120]

36. Akin-Ojo O, Song Y, Wang F. Developing ab Initio Quality Force Fields from Condensed Phase Quantum-Mechanics/Molecular-Mechanics Calculations through the Adaptive Force Matching Method. J. Chem. Phys. 2008; 129:064108. [PubMed: 18715052]

37. Wang, L-P. ForceBalance: Systematic Force Field Optimization. Stanford University; Mar. 2014 https://simtk.org/home/forcebalance/

38. Wang L-P, Chen J, van Voorhis T. Systematic Parametrization of Polarizable Force Fields from Quantum Chemistry Data. J. Chem. Theory Comput. 2013; 9:452–460. [PubMed: 26589047]

39. Wang L-P, Martinez TJ, Pande VS. Building Force Fields - An Automatic, Systematic, and Reproducible Approach. J. Phys. Chem. Lett. 2014; 5:1885–1891. [PubMed: 26273869]

40. Ren PY, Ponder JW. Polarizable Atomic Multipole Water Model for Molecular Mechanics Simulation. J. Phys. Chem. B. 2003; 107:5933–5947.

41. Ren P, Wu C, Ponder JW. Polarizable Atomic Multipole-based Molecular Mechanics for Organic Molecules. J. Chem. Theory Comput. 2011; 7:3143–3161. [PubMed: 22022236]

42. Shi Y, Xia Z, Zhang J, Best R, Wu C, Ponder JW, Ren P. The Polarizable Atomic Multipole-based AMOEBA Force Field for Proteins. J. Chem. Theory Comput. 2013; 9:4046–4063. [PubMed: 24163642]

43. Halgren TA. The Representation of van der Waals (vdW) Interactions in Molecular Mechanics Force Fields: Potential Form, Combination Rules, and vdW Parameters. J. Am. Chem. Soc. 1992; 114:7827–7843.

44. Thole BT. Molecular Polarizabilities Calculated with a Modified Dipole Interaction. Chem. Phys. 1981; 59:341–350.

45. Martyna GJ, Tuckerman ME, Tobias DJ, Klein ML. Explicit Reversible INtegrators for Extended Systems Dynamics. Mol. Phys. 1996; 87:1117–1157.

46. Ponder, JW. TINKER: Software Tools for Molecular Design, Version 7.0. Washington University in St. Louis; Jun. 2014 http://dasher.wustl.edu/tinker/

47. Eastman P, Friedrichs MS, Chodera JD, Radmer RJ, Bruns CM, Ku JP, Beauchamp KA, Lane TJ, Wang L-P, Shukla D, Tye T, Houston M, Stich T, Klein C, Shirts MR, Pande VS. OpenMM 4: A Reusable, Extensible, Hardware Independent Library for High Performance Molecular Simulation. J. Chem. Theory Comput. 2013; 9:461–469. [PubMed: 23316124]

48. Smith BJ, Swanton DJ, Pople JA, Schaefer HF, Radom L. Transition Structures for the Interchange of Hydrogen Atoms within the Water Dimer. J. Chem. Phys. 1990; 92:1240–1247.

49. Bates DM, Tschumper GS. CCSD(T) Complete Basis Set Limit Relative Energies for Low-Lying Water Hexamer Structures. J. Phys. Chem. A. 2009; 113(15):3555–3559. [PubMed: 19354314]

50. Xantheas SS, Apra E. The Binding Energies of the D2d and S4 Water Octamer Isomers: High-Level Electronic Structure and Empirical Potential Results. J. Chem. Phys. 2004; 120:823–828. [PubMed: 15267918]

51. Bulusu S, Yoo S, Apra E, Xantheas S, Zeng XC. Lowest-Energy Structures of Water Clusters (H2O)11 and (H2O)13. J. Phys. Chem. A. 2006; 110(42):11781–11784. [PubMed: 17048809]

52. Fanourgakis GS, Apra E, Xantheas SS. High-level ab Initio Calculations for the Four Low-Lying Families of Minima of (H2O)20. I. Estimates of MP2/CBS Binding Energies and Comparison with Empirical Potentials. J. Chem. Phys. 2004; 121:2655–2663. [PubMed: 15281866]

53. Fanourgakis GS, Apra E, de Jong WA, Xantheas SS. High-Level ab Initio Calculations for the Four Low-Lying Families of Minima of (H2O)20. II. Spectroscopic Signatures of the Dodecahedron, Fused Cubes, Face-Sharing Pentagonal Prisms, and Edge-Sharing Pentagonal Prisms Hydrogen Bonding Networks. J. Chem. Phys. 2005; 122:134304. [PubMed: 15847462]

54. Wang LP, Head-Gordon T, Ponder JW, Ren P, Chodera JD, Eastman PK, Martinez TJ, Pande VS. Systematic Improvement of a Classical Molecular Model of Water. J. Phys. Chem. B. 2013; 117:9956–9972. [PubMed: 23750713]

55. Steele RP, DiStasio RA Jr. Shao Y, Kong J, Head-Gordon M. Dual-Basis Second-Order Moller-Plesset Perturbation Theory: A Reduced-Cost Reference for Correlation Calculations. J. Chem. Phys. 2006; 125:074108. [PubMed: 16942323]

56. Steele RP, DiStasio RA, Head-Gordon M. Non-Covalent Interactions with Dual-Basis Methods: Pairings for Augmented Basis Sets. J. Chem. Theory Comput. 2009; 5:1560–1572. [PubMed: 26609849]

57. Dunning TH. Gaussian Basis Sets for Use in Correlated Molecular Calculations. I. The Atoms Boron through Neon and Hydrogen. J. Chem. Phys. 1989; 90:1007–1023.

58. Shao Y, Molnar LF, Jung Y, Kussmann J, Ochsenfeld C, Brown ST, Gilbert AT, Slipchenko LV, Levchenko SV, O'Neill DP, DiStasio RA Jr. Lochan RC, Wang T, Beran GJ, Besley NA, Herbert JM, Lin CY, Van Voorhis T, Chien SH, Sodt A, Steele RP, Rassolov VA, Maslen PE, Korambath PP, Adamson RD, Austin B, Baker J, Byrd EF, Dachsel H, Doerksen RJ, Dreuw A, Dunietz BD, Dutoi AD, Furlani TR, Gwaltney SR, Heyden A, Hirata S, Hsu CP, Kedziora G, Khalliulin RZ, Klunzinger P, Lee AM, Lee MS, Liang W, Lotan I, Nair N, Peters B, Proynov EI, Pieniazek PA, Rhee YM, Ritchie J, Rosta E, Sherrill CD, Simmonett AC, Subotnik JE, Woodcock HL 3rd, Zhang W, Bell AT, Chakraborty AK, Chipman DM, Keil FJ, Warshel A, Hehre WJ, Schaefer HF 3rd, Kong J, Krylov AI, Gill PM, Head-Gordon M. Advances in Methods and Algorithms in a Modern Quantum Chemistry Program Package. Phys. Chem. Chem. Phys. 2006; 8:3172–3191. [PubMed: 16902710]

59. Ren PY, Ponder JW. Temperature and Pressure Dependence of the AMOEBA Water Model. J. Phys. Chem. B. 2004; 108:13427–13437.

60. Levenberg K. A Method for the Solution of Certain Non-Linear Problems in Least Squares. Q. Appl. Math. 1944; 2:164–168.

61. Marquardt DW. An Algorithm for Least-Squares Estimation of Nonlinear Parameters. J. Soc. Ind. Appl. Math. 1963; 11:431–441.

62. Dennis JE, Gay DM, Welsch RE. An Adaptive Non-Linear Least-Squares Algorithm. ACM T. Math. Software. 1981; 7:348–368.

63. More JJ, Sorensen DC. Computing a Trust Region. SIAMJ. Sci. Stat. Comp. 1983; 4:553–572.

64. Di Pierro M, Elber R. Automated Optimization of Potential Parameters. J. Chem. Theory Comput. 2013; 9:3311–3320. [PubMed: 24015115]

65. Bui, P.; Rajan, D.; Abdul-Wahid, B.; Izaguirre, JA.; Thain, D. Work Queue + Python: A Framework For Scalable Scientific Ensemble Applications; Workshop on Python for High Performance and Scientific Computing (PyHPC); Seattle WA. Nov. 2011;

66. Shirts MR, Chodera JD. Statistically Optimal Analysis of Samples from Multiple Equilibrium States. J. Chem. Phys. 2008; 129:124105. [PubMed: 19045004]

67. Millot C, Soetens J-C, Martins Costa MT, Hodges MP, Stone AJ. Revised Anisotropic Site Potentials for the Water Dimer and Calculated Properties. J. Phys. Chem. A. 1998; 102:754–770.

68. Benjamin KM, Schultz AJ, Kofke DA. Virial Coefficients of Polarizable Water Applications to Thermodynamic Properties and Molecular Clustering. J. Phys. Chem. C. 2007; 111:16021–16027.

69. Bustos Marun RA, Coronado EA, Ferrero JC. Second Virial Coefficients of Water Beyond the Conventional First-Order Quantum Correction. Chem. Phys. Lett. 2005; 405:203–207.

70. Nymand TM, Astrand PO. Calculation of the Geometry of the Water Molecule in Liquid Water. J. Phys. Chem. A. 1997; 101:10039–10044.

71. Ichikawa K, Kameda Y, Yamaguchi T, Wakita H, Misawa M. Neutron-Diffraction Investigation of the Intramolecular Structure of a Water Molecule in the Liquid-Phase at High-Temperatures. Mol. Phys. 1991; 73:79–86.

72. Debenedetti PG, Stanley HE. Supercooled and Glassy Water. Physics Today. Jun.2003 :40–46.

73. Carnie SL, Patey GN. Fluids of Polarizable Hard-Spheres with Dipoles and Tetrahedral Quadrupoles- Integral-Equation Results with Application to Liquid Water. Mol. Phys. 1982; 47:1129–1151.

74. Head-Gordon T, Rick SW. Consequences of Chain Networks on Thermodynamic, Dielectric and Structural Properties for Liquid Water. Phys. Chem. Chem. Phys. 2007; 9:83–91. [PubMed: 17164889]

75. Soper AK, Phillips MG. A New Determination of the Structure of Water at 25-Degrees-C. Chem. Phys. 1986; 107:47–60.

76. Soper AK. The Radial Distribution Functions of Water and Ice from 220 to 673 K and at Pressures up to 400 MPa. Chem. Phys. 2000; 258:121–137.

77. Sorenson JM, Hura G, Glaeser RM, Head-Gordon T. What Can X-ray Scattering Tell Us about the Radial Distribution Functions of Water? J. Chem. Phys. 2000; 113:9149–9161.

78. Skinner LB, Huang C, Schlesinger D, Pettersson LG, Nilsson A, Benmore CJ. Benchmark Oxygen-Oxygen Pair-Distribution Function of Ambient Water from X-ray Diffraction Measurements with a Wide Q-Range. J. Chem. Phys. 2013; 138:074506. [PubMed: 23445023]

79. Hura G, Sorenson JM, Glaeser RM, Head-Gordon T. A High-Quality X-Ray Scattering Experiment on Liquid Water at Ambient Conditions. J. Chem. Phys. 2000; 113:9140–9148.

80. Morita A. Water Polarizability in Condensed Phase: Ab Initio Evaluation by Cluster Approach. J. Comput. Chem. 2002; 23:1466–1471. [PubMed: 12370948]

81. Salanne M, Vuilleumier R, Madden PA, Simon C, Turq P, Guillot B. Polarizabilities of Individual Molecules and Ions in Liquids from First Principles. J. Phys.-Condens. Mat. 2008; 20:494207.

82. Harris KR, Woolf LA. Temperature and Volume Dependence of the Viscosity of Water and Heavy Water at Low Temperature. J. Chem. Phys. Ref. Data. 2004; 49:1064–1069.

83. Yeh I-C, Hummer G. System-Size Dependence of Diffusion Coefficients and Viscosities from Molecular Dynamics Simulations with Periodic Boundary Conditions. J. Phys. Chem. B. 2004; 108:15873–15879.

84. White HJ, Sengers JV, Neumann DB, Bellows JC. IAPWS Release on the Surface Tension of Ordinary Water Substance. 1995

85. Zheng L, Chen M, Yang W. Random Walk in Orthogonal Space to Achieve Efficient Free-Energy Simulation of Complex Systems. Proc. Natl. Acad. Sci. USA. 2008; 105:20227–20232. [PubMed: 19075242]

86. Guillot B, Guissani Y. How to Build a Better Pair Potential for Water. J. Chem. Phys. 2001; 114:6720–6733.

87. Piquemal J-P, Gresh N, Giessner-Prettre C. Improved Formulas for the Calculation of the Electrostatic Contribution to the Intermolecular Interaction Energy from Multipolar Expansion of the Electronic Distribution. J. Phys. Chem. A. 2003; 107:10353–10359. [PubMed: 26313624]

88. Wang B, Truhlar DG. Screened Electrostatic Interactions in Molecular Mechanics. J. Chem. Theory Comput. 2014; 10:4480–4487. [PubMed: 26588144]

89. Tafipolsky M, Engels B. Accurate Intermolecular Potentials with Physically Grounded Electrostatics. J. Chem. Theory Comput. 2011; 7:1791–1803. [PubMed: 26596442]

90. Freitag MA, Gordon MS, Jansen JH, Stevens WJ. Evaluation of Charge Penetration between Distributed Multipolar Expansions. J. Chem. Phys. 2000; 112:7300–7306.

91. Slipchenko LV, Gordon MS. Electrostatic Energy in the Effective Fragment Potential Method: Theory and Application to Benzene Dimer. J. Comput. Chem. 2006; 28:276–291. [PubMed: 17143863]

92. Clough SA, Beers Y, Klein GP, Rothman LS. Dipole-Moment of Water from Stark Measurements of H2O, HDO, and D2O. J. Chem. Phys. 1973; 59:2254–2259.

93. Verhoeven J, Dymanus A. Magnetic Properties and Molecular Quadrupole Tensor of the Water Molecule by Beam-Maser Zeeman Spectroscopy. J. Chem. Phys. 1970; 52:3222–3233.

94. Murphy WF. The Rayleigh Depolarization Ratio and Rotational Raman Spectrum of Water Vapor and the Polarizability Components for the Water Molecule. J. Chem. Phys. 1977; 67:5877–5882.

95. Curtiss LA, Frurip DJ, Blander M. Studies of Molecular Association in H2O and D2O Vapors by Measurement of Thermal Conductivity. J. Chem. Phys. 1979; 71:2703–2711.

96. Odutola JA, Dyke TR. Partially Deuterated Water Dimers - Microwave-Spectra and Structure. J. Chem. Phys. 1980; 72:5062–5070.

97. Tschumper GS, Leininger ML, Hoffman BC, Valeev EF, Schaefer HF, Quack M. Anchoring the Water Dimer Potential Energy Surface with Explicitly Correlated Computations and Focal Point Analyses. J. Chem. Phys. 2002; 116:690–701.

98. Klopper W, van Duijneveldt-van de Rijdt JGCM, van Duijneveldt FB. Computational Determination of Equilibrium Geometry and Dissociation Energy of the Water Dimer. Phys. Chem. Chem. Phys. 2000; 2:2227–2234.

99. Lee HM, Suh SB, Lee JY, Tarakeshwar P, Kim KS. Structures, Energies, Vibrational Spectra, and Electronic Properties of Water Monomer to Decamer. J. Chem. Phys. 2000; 112:9759–9772.

100. van Duijneveldt-van de Rijdt JGCM, Mooij WTM, van Duijneveldt FB. Testing the Quality of Some Recent Water-Water Potentials. Phys. Chem. Chem. Phys. 2003; 5:1169–1180.

101. Yoo S, Aprà E, Zeng XC, Xantheas SS. High-Level Ab Initio Electronic Structure Calculations of Water Clusters (H2O)16 and (H2O)17: A New Global Minimum for (H2O)16. J. Phys. Chem. Lett. 2010; 1:3122–3127.

102. Wagner W, Pruss A. The IAPWS Formulation 1995 for the Thermodynamic Properties of Ordinary Water Substance for General and Scientific Use. J. Phys. Chem. Ref. Data. 2002; 31:387–535.

103. Schmid R, Miah AM, Sapunov VN. A New Table of the Thermodynamic Quantities of Ionic Hydration: Values and Some Applications. Phys. Chem. Chem. Phys. 2000; 2:97–102.

104. Feller D, Glendening ED, Woon DE, Feyereisen MW. An Extended Basis-Set Ab-Initio Study of Alkali-Metal Cation-Water Clusters. J. Chem. Phys. 1995; 103:3526–3542.

105. Xantheas SS. Quantitative Description of Hydrogen Bonding in Chloride-Water Clusters. J. Phys. Chem. 1996; 100:9703–9713.

106. Lide, DR. CRC Handbook of Chemistry and Physics. 82nd. CRC Press LLC; Boca Raton, FL: 2001.

107. Kell GS, McLaurin GE, Whalley E. PVT Properties of Water VII. Vapour Densities of Light and Heavy Water from 150 to 500 C. P. R Soc. A. 1989; 425:49–71.

108. Kell GS. Density, Thermal Expansivity, and Compressibility of Liquid Water from 0 deg. to 150 deg. Correlations and Tables for Atmospheric Pressure and Saturation Reviewed and Expressed on 1968 Temperature Scale. J. Chem. Phys. Ref. Data. 1975; 20:97–105.
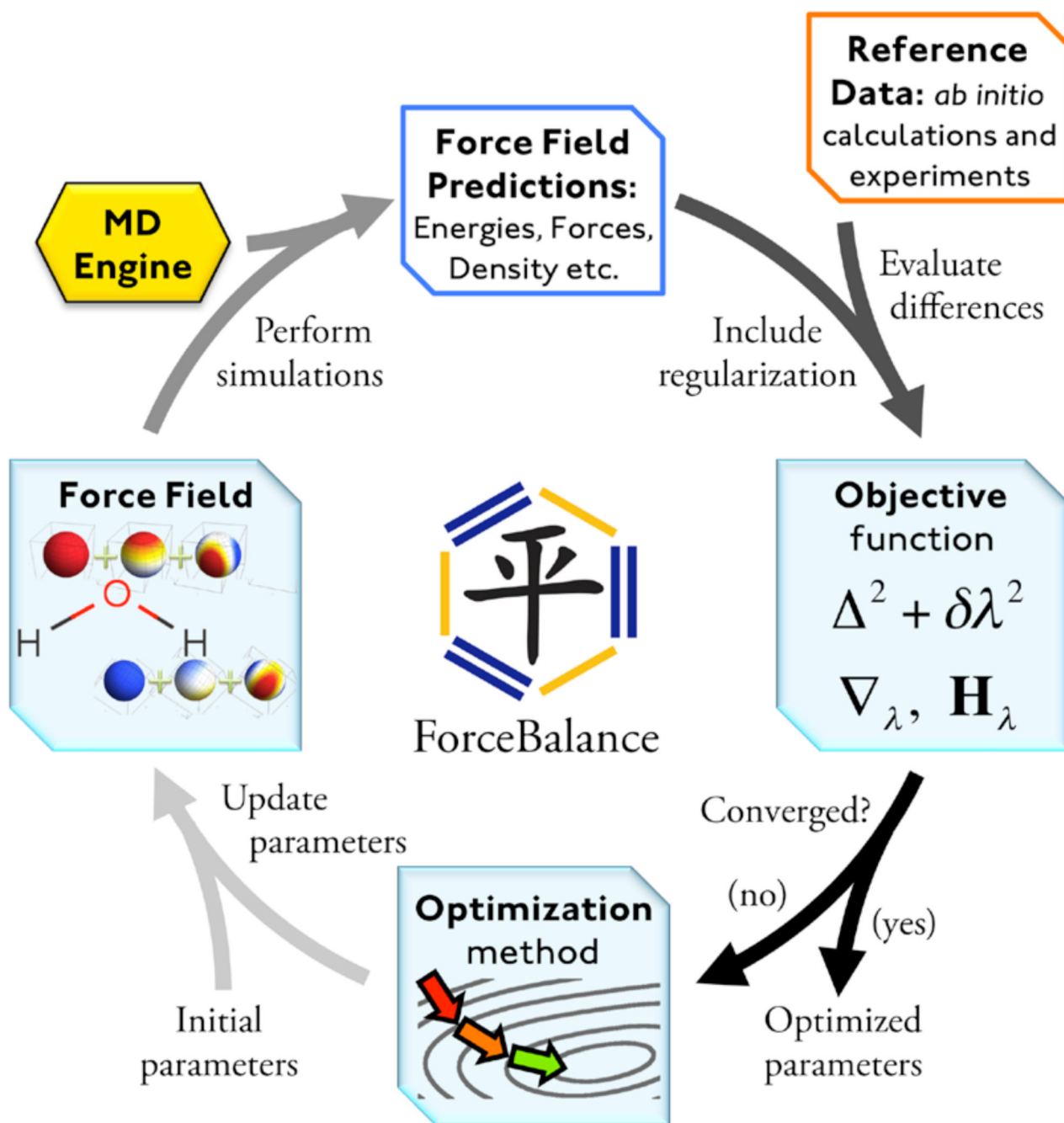
Figure 1.
The ForceBalance procedure. Calculation begins with an initial set of parameters (lower left), which is used to generate a force field and perform simulations (upper left). The objective function is a weighted sum of squared differences between the simulation results and the reference data (right), plus a regularization term used to prevent overfitting. The optimization method (bottom) updates the parameters in order to minimize the objective function.
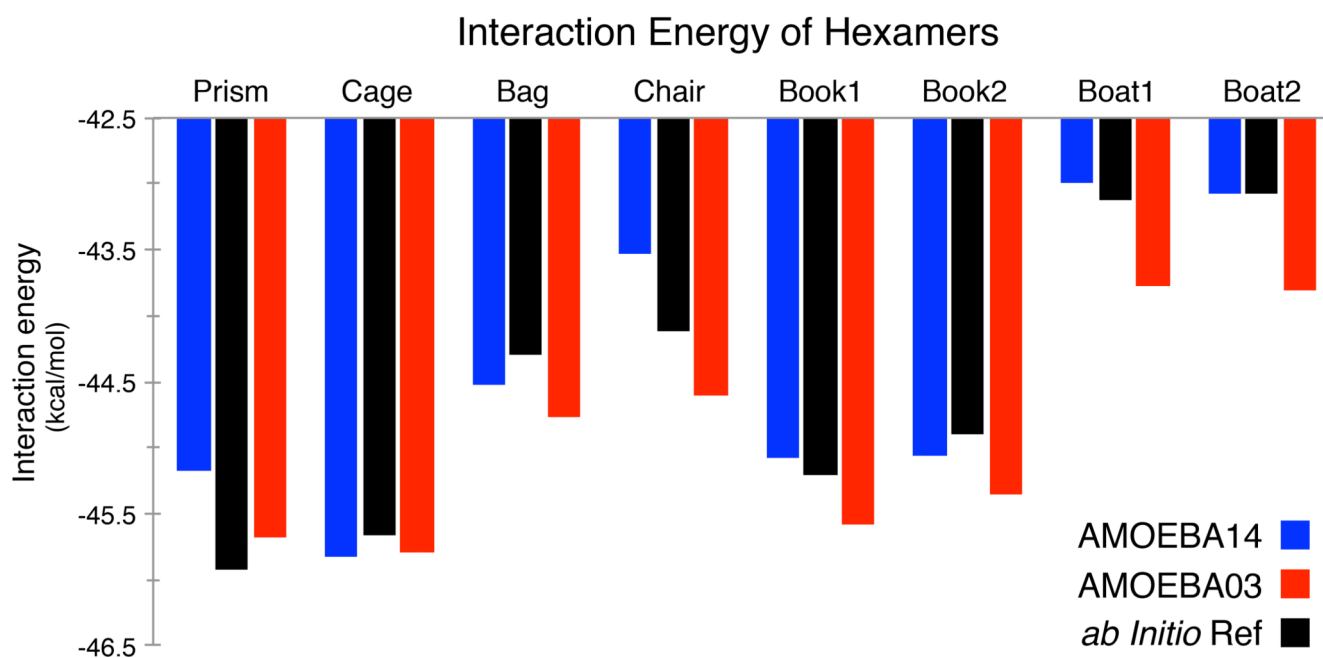
Figure 2.
Energies of water hexamer minima for the AMOEBA03 and AMOEBA14 models compared to reference complete basis set (CBS) *ab initio* calculations from Reference 49.
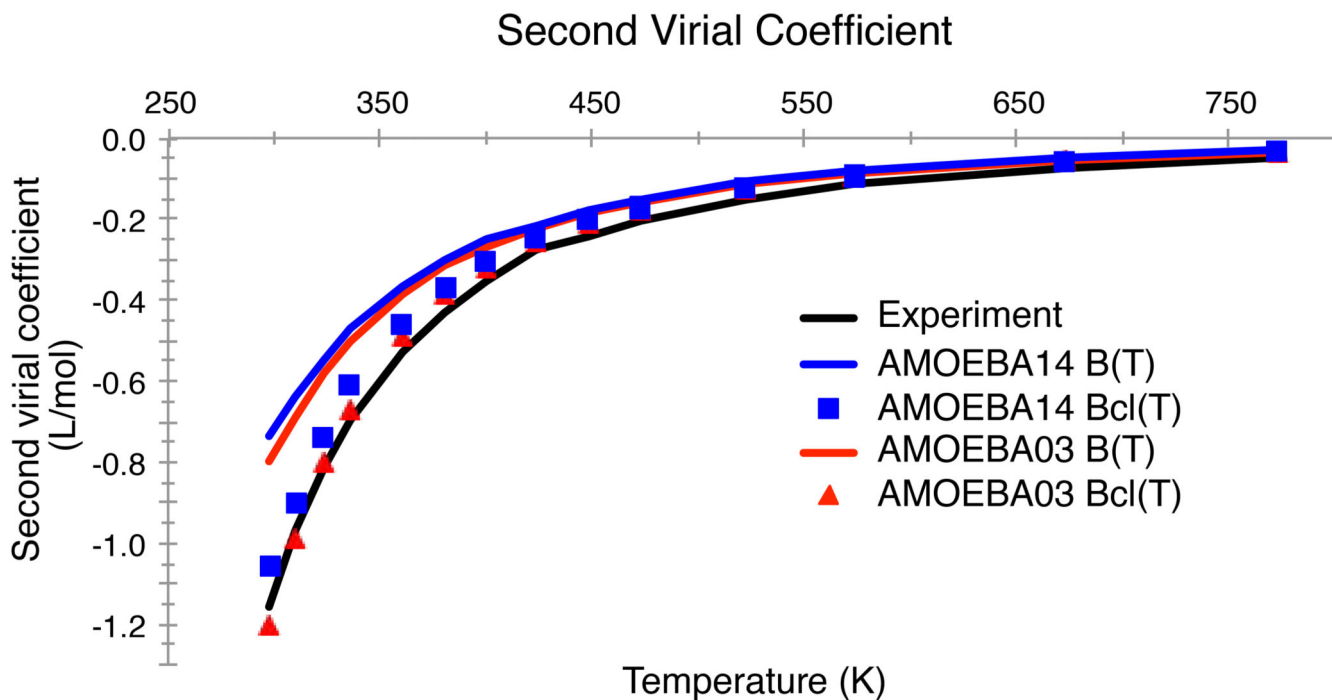
Figure 3.
Second virial coefficient of water as a function of temperature for the AMOEBA03 and AMOEBA14 models for temperatures from 249 K to 373 K and atmospheric pressure (1 atm). The Bcl(T) curves show the classical second virial coefficient, while the B(T) curves have translational and rotational quantum corrections added to the classical results. Experimental values are from References 106 and 107.

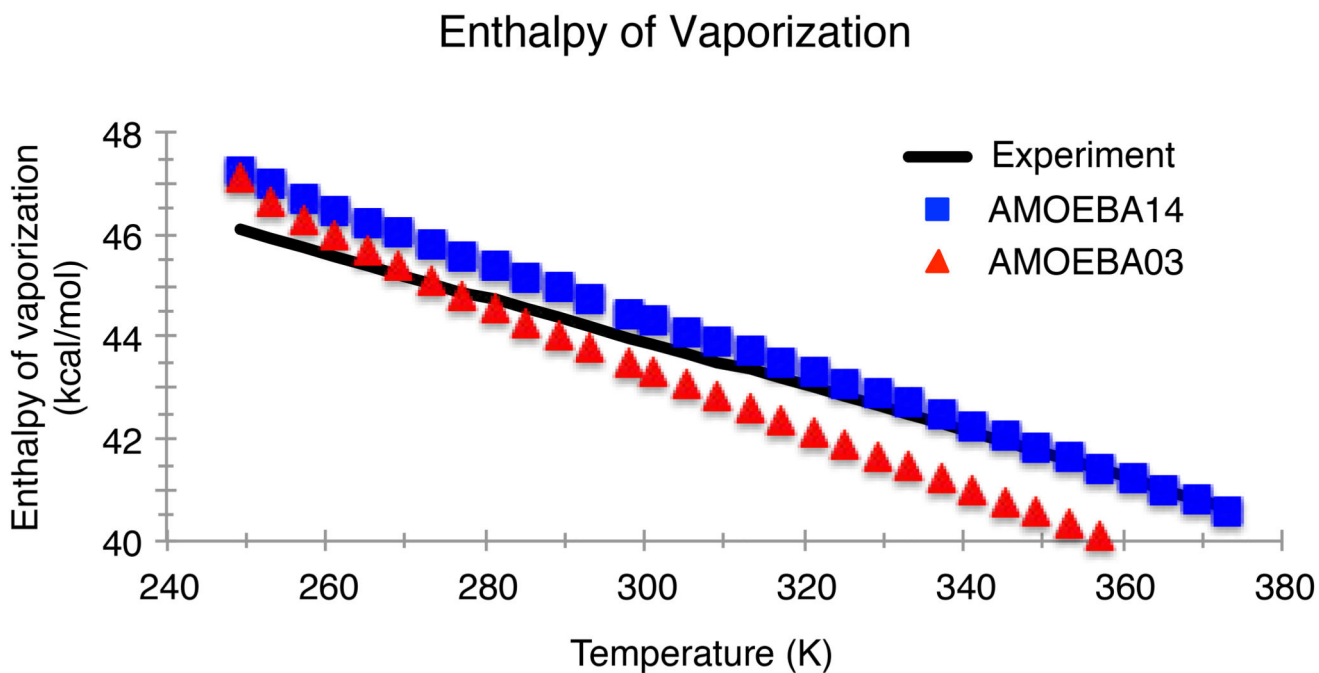## Enthalpy of Vaporization

Figure 4.
Enthalpy of vaporization of water for temperatures for the AMOEBA03 and AMOEBA14 models and experiment for temperatures from 249 K to 373 K and atmospheric pressure (1 atm). The mean signed deviation is −0.43 kcal/mol. Experimental values are from Reference 102.

Figure 5.
Density of water for the AMOEBA03 and AMOEBA14 models compared to experiment for temperatures from 249 K to 373 K at atmospheric pressure (1 atm). The temperature of maximum density from experiment and for AMOEBA14 is 277 K. Experimental values are taken from Reference 108.

Isobaric Heat Capacity

Figure 6.
Isobaric heat capacity for the AMOEBA03 and AMOEBA14 models compared to experiment for temperatures from 249 K to 373 K at atmospheric pressure (1 atm). Experimental values are taken from Reference 102.

Figure 7.
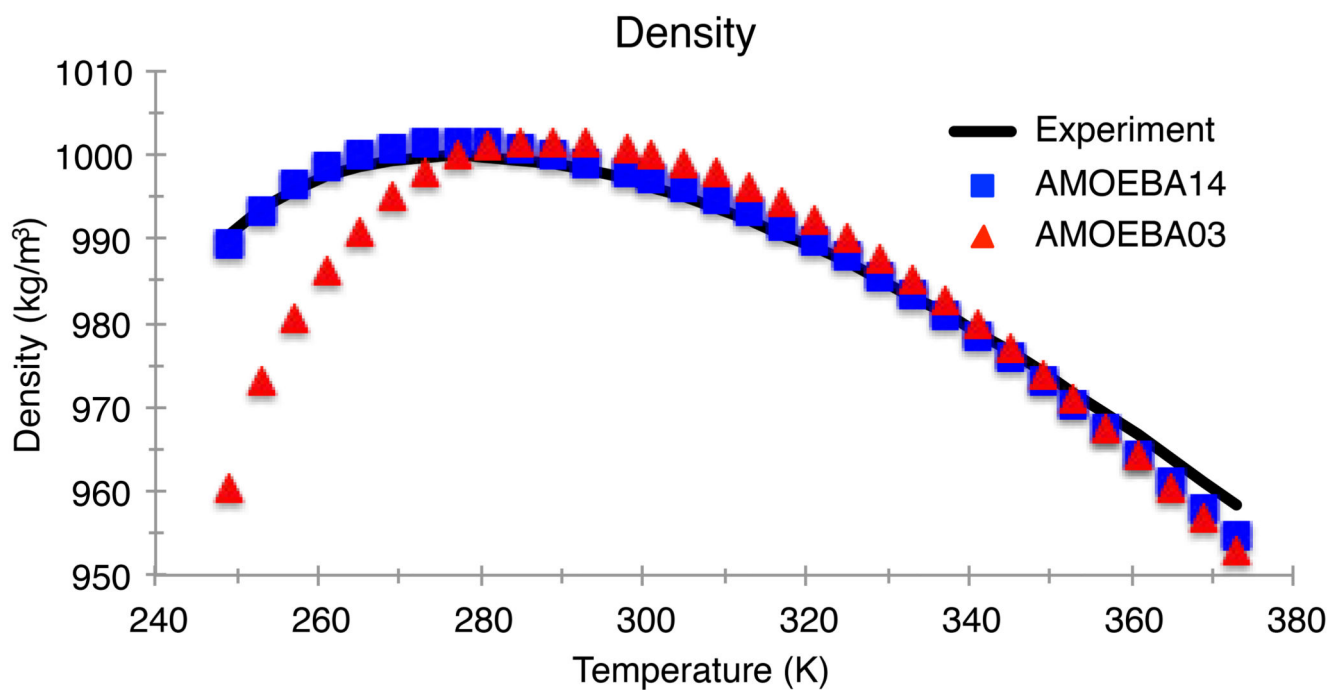Isothermal compressibility for the AMOEBA03 and AMOEBA14 models compared to
experiment for temperatures from 249 K to 373 K at atmospheric pressure (1 atm).
Experimental values taken from Reference 108.
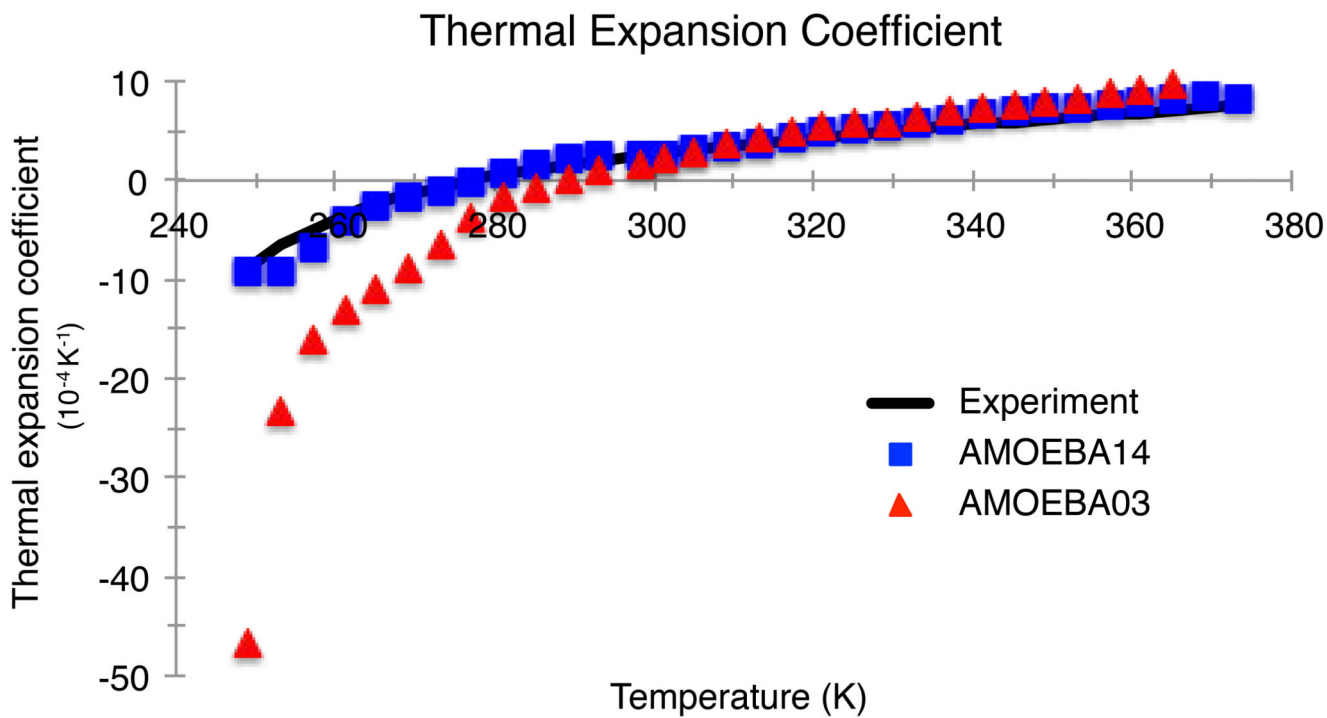
Figure 8.
Thermal expansion coefficient for the AMOEBA03 and AMOEBA14 models compared to experiment for temperatures from 249.15K to 373.15K at atmospheric pressure (1 atm). Experimental values are from Reference 108.
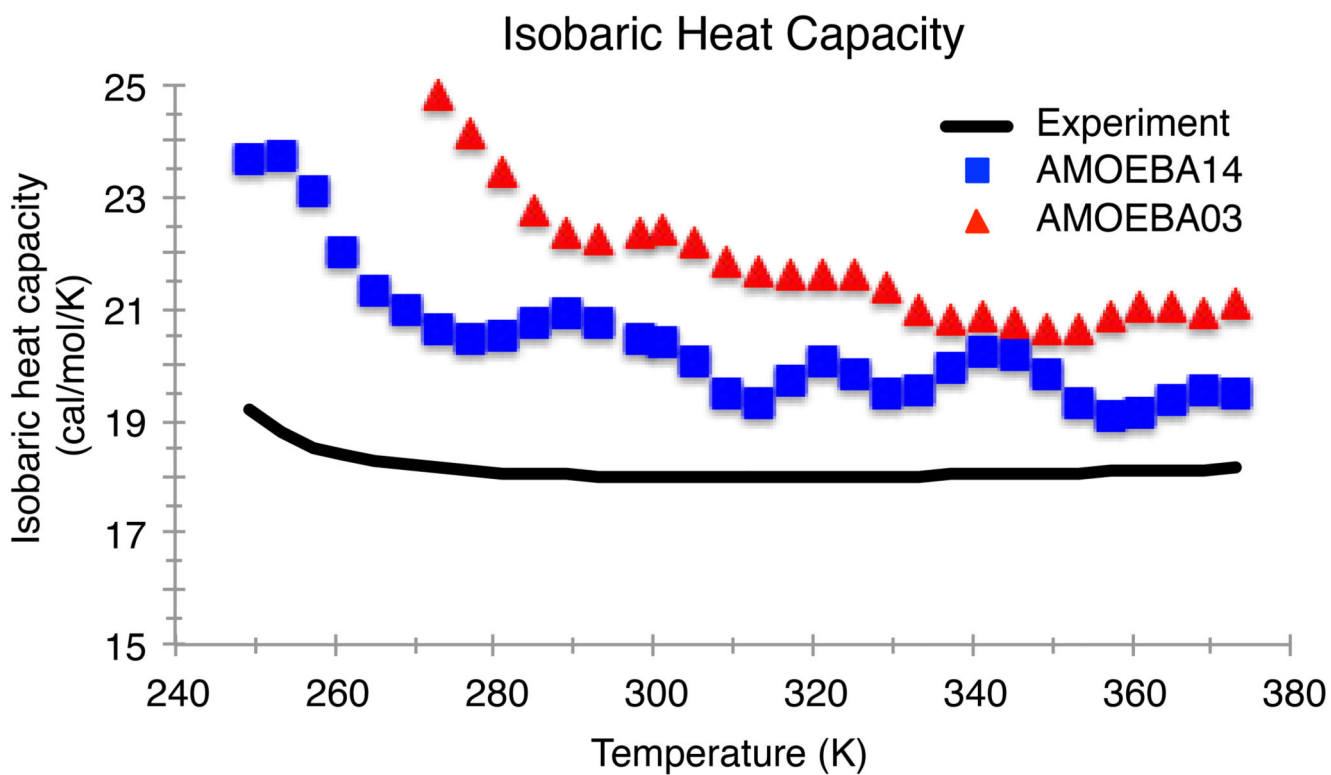
Dielectric Constant
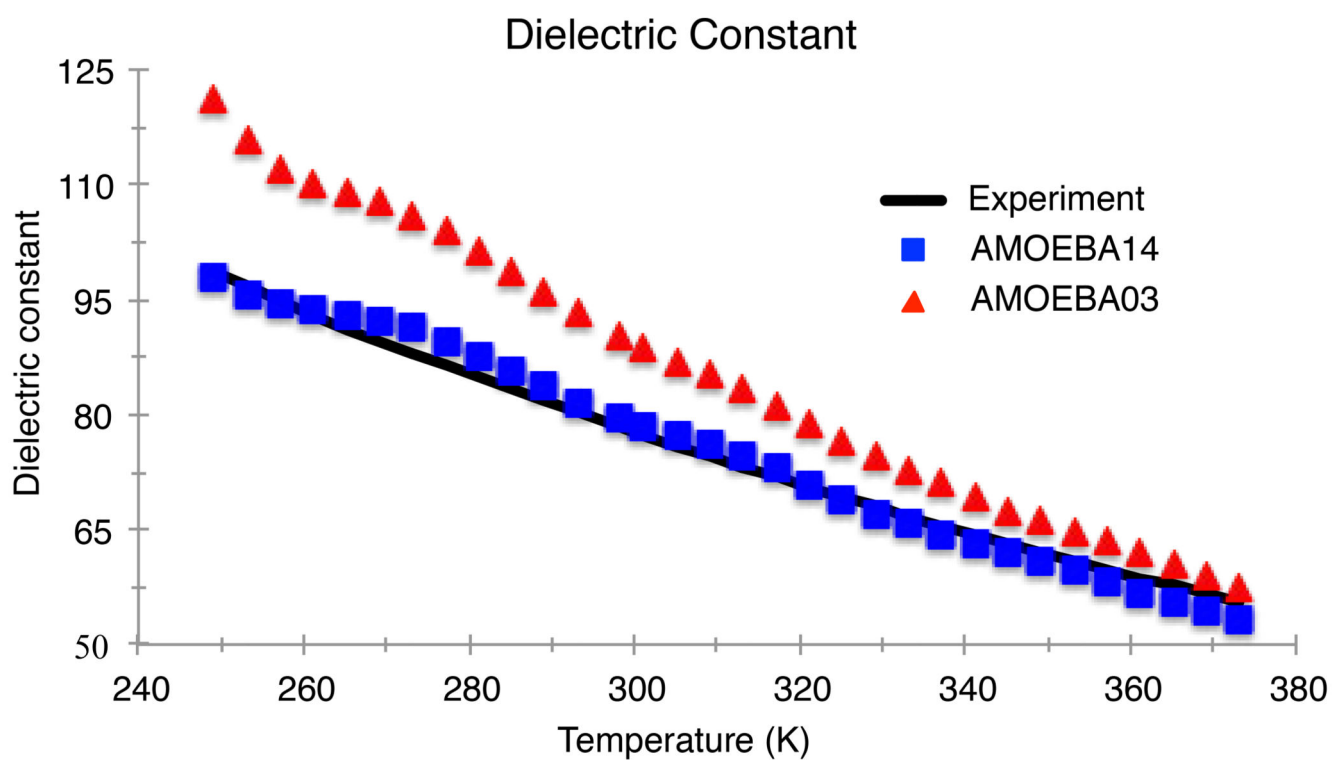
Figure 9.
Dielectric constant for the AMOEBA03 and AMOEBA14 models compared to experiment. For temperatures from 249 K to 373 K at atmospheric pressure (1 atm). Experimental values are taken from Reference 102.
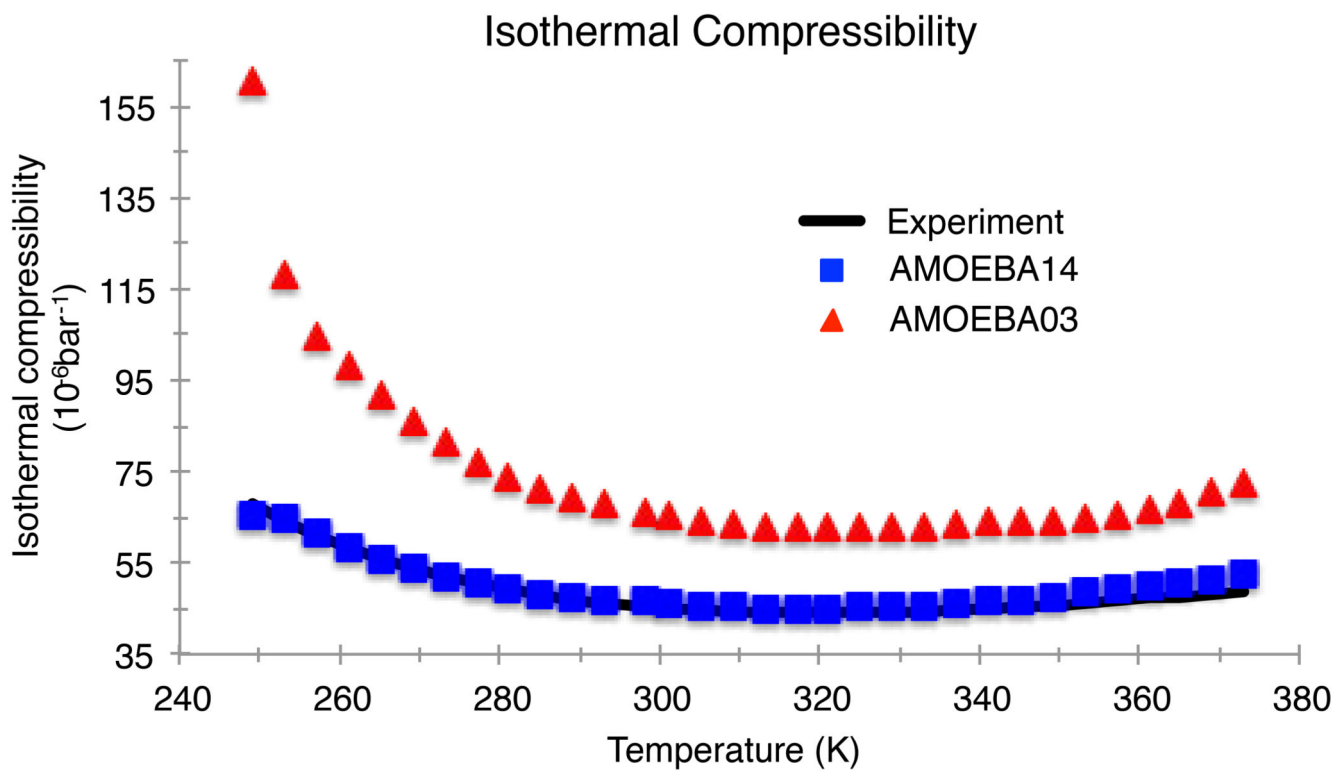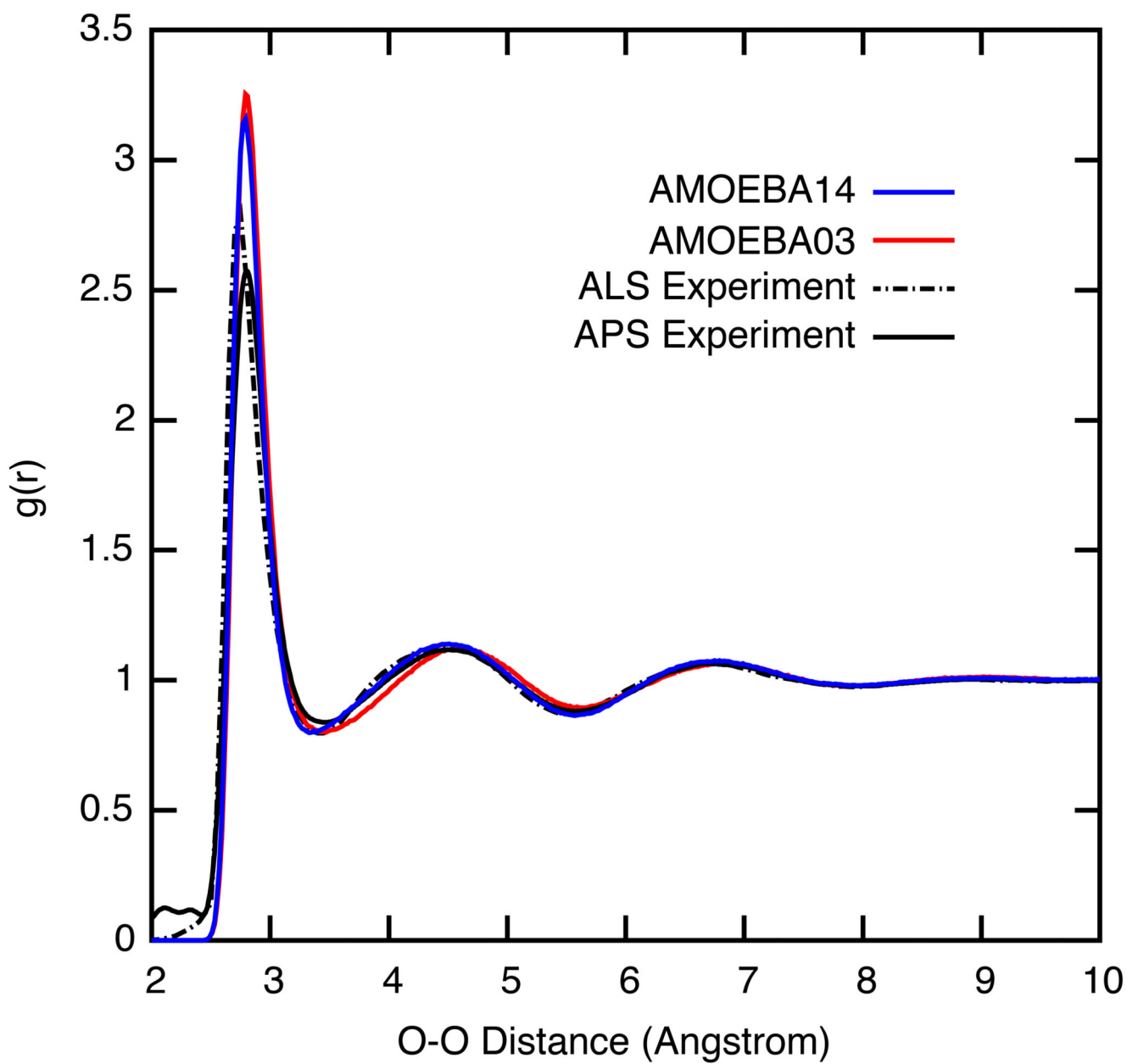
Figure 10.
The water oxygen-oxygen radial distribution functions at 298 K for AMOEBA03,
AMOEBA14 and iAMOEBA compared against experimental values from References 77-79.
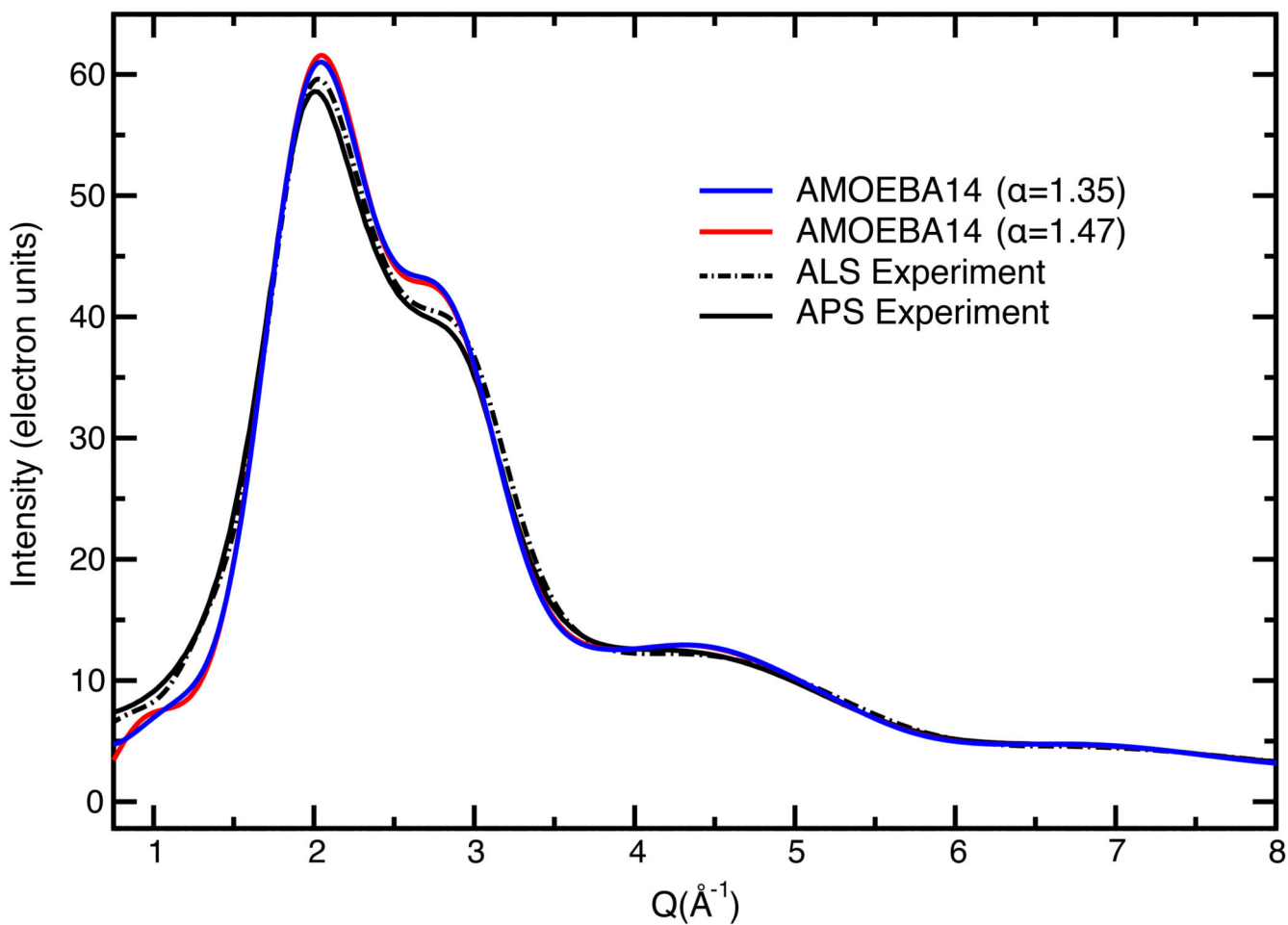
Figure 11.
Comparison of the ALS and APS experimental X-ray scattering intensities from References 78 and 79 for liquid water at 1 bar and 298 K with curves simulated with AMOEBA14 models modified to have molecular polarizabilities of $\alpha=1.47$ $\mathring{A}^3$ and $\alpha=1.35$ $\mathring{A}^3$.

Table 1

AMOEBA water parameters for the AMOEBA03 and revised AMOEBA14 water models and the prior widths used in the ForceBalance optimization scheme.

| Parameter	Units	AMOEBA03	AMOEBA14	Prior Width
O Monopole	e	–0.51966	–0.42616	0.4
O Dipole Z	e bohr	0.14279	0.06251	0.1
O Quadrupole XX	e bohr^2	0.37928	0.17576	0.2
O Quadrupole YY	e bohr^2	–0.41809	–0.23160	0.2
O Quadrupole ZZ	e bohr^2	0.03881	0.05584	0.2
H Monopole	e	0.25983	0.21308	0.4
H Dipole X	e bohr	–0.03859	–0.10117	0.1
H Dipole Z	e bohr	–0.05818	–0.27171	0.1
H Quadrupole XX	e bohr^2	–0.03673	0.12283	0.2
H Quadrupole YY	e bohr^2	–0.10739	0.08950	0.2
H Quadrupole XZ	e bohr^2	–0.00203	–0.06989	0.2
H Quadrupole ZZ	e bohr^2	0.14412	–0.21233	0.2
O Polarizability	Å	0.837	0.920	0.1
H Polarizability	Å	0.496	0.539	0.1
Damping Factor	Å	0.39	0.39	none
O vdW Diameter	Å	3.405	3.5791	0.3
O vdW Epsilon	kcal/mol	0.11	0.1512	0.1
H vdW Diameter	Å	2.655	2.1176	0.3
H vdW Epsilon	kcal/mol	0.0135	0.0105	0.1
H vdW Reduction Factor	none	0.91	0.8028	0.1
O-H Bond Length	Å	0.9572	0.9565	0.1
Bond Force Constant	kcal/mol/Å^2	556.85[a]	556.82	50
H-O-H Angle Value	degree	108.5	107.91	5
Angle Force Constant	kcal/mol/rad^2	48.7[a]	48.98	40
H-H Urey-Bradley Length	Å	1.5326[a]	1.5467	none
Urey-Bradley Force Const.	kcal/mol/Å^2	–7.6[a]	–8.62	25

[a]Current AMOEBA03 bond angle and Urey-Bradley intramolecular parameters. These values differ from those originally published in Reference 40, and were changed to correct an error in the ordering of the O-H stretch vibrational modes.

Table 2

Multipole properties predicted by the revised AMOEBA14 and previous AMOEBA03 water models compared to experimental values. Units are Debye, Debye·A, and $A^2 \cdot s^4 \cdot kg^{-1}$, respectively.

	AMOEBA03	AMOEBA14	Experiment
Dipole d_z	1.771	1.808	1.855[a]
Quadrupole			
$\mathbf{Q}_{xx}$	2.502	2.626	2.630[b]
$\mathbf{Q}_{yy}$	−2.168	−2.178	−2.500[b]
$\mathbf{Q}_{zz}$	−0.334	−0.045	−0.130[b]
Polarizability			
$\mathbf{\alpha}_{xx}$	1.672	1.767	1.528[c]
$\mathbf{\alpha}_{yy}$	1.225	1.308	1.412[c]
$\mathbf{\alpha}_{zz}$	1.328	1.420	1.468[c]

[a] Reference 92.

[b] Reference 93.

[c] Reference 94.

Table 3

Dimer equilibrium properties: Dissociation energy (D_e, kcal/mol), O-O distance (r_{O-O}, Å), α angle (angle between O-O vector and O_{donor}-H_{donor} vector, degrees), β angle (angle between O-O vector and plane of acceptor molecule, degrees), total dipole moment (μ_{tot}, Debye).

Property	AMOEBA03	AMOEBA14	*ab Initio*	Experiment
De	4.96	4.64	4.98[c]	5.44±0.7[a]
r $_{O-O}$	2.892	2.908	2.907[c]	2.976[b]
α	4.18	4.41	4.18[c]	−1±10[b]
β	57.2	64.9	55.6[d]	57±10[b]
μ $_{tot}$	2.54	2.20	2.76[e]	2.643[b]

[a]Reference 95.

[b]Reference 96.

[c]Reference 97.

[d]Reference 98.

[e]Reference 99.

Table 4

Cluster binding energies (kcal/mol) with the AMOEBA14 model in comparison to *ab initio* reference calculations. Mean absolute deviations (MADs) are reported over the small and large cluster categories.

Molecule		Ref.	AMOEBA14	Diff.
	1	−4.968	−4.65	0.32
	2	−4.453	−4.22	0.24
	3	−4.418	−4.19	0.23
	4	−4.25	−3.54	0.71
Dimers [a] (Smith)	5	−3.998	−3.06	0.94
	6	−3.957	−2.92	1.04
	7	−3.256	−2.49	0.77
	8	−1.3	−1.02	0.28
	9	−3.047	−2.37	0.68
	10	−2.182	−1.96	0.22
Trimer [b]		−15.742	−15.38	0.36
Tetramer [b]		−27.4	−27.43	−0.03
Pentamer [b]		−35.933	−35.78	0.16
	Prism	−45.92	−45.18	0.74
	Cage	−45.67	−45.83	−0.16
	Bag	−44.3	−44.52	−0.22
	CyclicChair	−44.12	−43.53	0.59
Hexamer [c]	Book A	−45.2	−45.08	0.12
	Book B	−44.9	−45.06	−0.16
	CyclicBoat A	−43.13	−42.99	0.14
	CyclicBoat B	−43.07	−43.07	0.00
Octamer [d]	S_4	−72.7	−72.22	0.48
	D_{2d}	−72.7	−72.24	0.46
11-mer [e]	434	−105.718	−101.11	4.61

Molecule		Ref.	AMOEBA14	Diff.
	515	−105.182	−100.99	4.19
	551	−104.92	−100.58	4.34
	443	−104.76	−101.17	3.59
	4412	−103.971	−100.33	3.64
	Boat A	−170.8	−160.45	10.35
	Boat B	−170.63	−160.39	10.25
16-mer[f]	Anti-boat	−170.54	−160.30	10.25
	ABAB	−171.05	−161.20	9.85
	AABB	−170.51	−160.89	9.62
17-mer[f]	Sphere	−182.54	−171.53	11.01
	5525	−181.83	−170.42	11.41
	Dodecahedron	−200.1	−193.81	6.29
20-mer[g]	FusedCubes	−212.1	−205.77	6.33
	FaceSharingPrisms	−215.2	−204.41	10.79
	EdgeSharingPrisms	−218.1	−207.06	11.04
		MAD	Units	
Clusters	Dimer to Octamer	0.39	kcal/mol	
	11- to 20-mer	7.97	kcal/mol	

[a] Reference 100.

[b] Reference 40.

[c] Reference 49.

[d] Reference 50.

[e] Reference 51.

[f] Reference 101.

[g] Reference 52.

Table 5

Mean absolute deviations (MADs) from experiment of the liquid phase properties calculated by AMOEBA14 across all temperatures (249K to 373K).

Property	MAD	Units
ρ	1.22	kg/m^3
H_{vap}	0.43	kJ/mol
α	0.66	$10^{-4}/K$
κ_T	1.31	$10^{-6}/bar$
C_p	2.28	$cal/mol/K$
$\varepsilon(0)$	1.51	N/A

Table 6

Miscellaneous bulk water properties and ion solvation free energies for the AMOEBA14 water model. All energies are in kcal/mol. Distances are in Å, viscosity in cP, and diffusion is in 10^{-5} cm^2/s.

Property	Expt	AMOEBA03	AMOEBA14	iAMOEBA
Viscosity	0.896[b]	1.08	0.900	0.85
Self-Diffusion Constant	2.29[c]	2.0	1.99	2.54
Size-Corrected Diffusion[a]	—	2.3	2.36	2.93
Surface Tension (300K)	71.73[d]	64	—	68.3
Surface Tension (298K)	71.97[d]	—	69.21	—
Na$^+$ G(Hydration)	−86.8[e]	−89.9	−91.91	—
Cl$^-$ G(Hydration)	−87.2[e]	−84.6	−89.25	—
Na$^+$-H$_2$O Dimer Distance	2.23[f]	2.232	2.252	2.47
Na$^+$-H$_2$O Dissociation Energy	−23.6[f]	−23.53	−23.23	−21.81
Cl$^-$-H$_2$O Dimer Distance	3.103[g]	3.151	3.147	2.965
Cl$^-$-H$_2$O Dissociation Energy	−15.4[g]	−15.99	−15.72	−18.11

[a]Reference 83.

[b]Reference 82.

[c]Reference 102.

[d]Reference 84.

[e]Reference 103.

[f]Reference 104.

[g]Reference 105.